KENTUCKY GEOLOGICAL SURVEY
Donald C. Haney, State Geologist and Director
UNIVERSITY OF KENTUCKY, LEXINGTON

HYDROGEOLOGY, HYDROGEOCHEMISTRY, AND SPOIL SETTLEMENT AT A LARGE MINE-SPOIL AREA IN EASTERN KENTUCKY: STAR FIRE TRACT

David R. Wunsch, James S. Dinger, Page B. Taylor, Daniel I. Carey, and C. Douglas R. Graham

REPORT OF INVESTIGATIONS 10 Series XI, 1996

DISCLAIMER

The Kentucky Geological Survey provides online versions of its publications as a public service. Publications are provided as Adobe PDF (portable document format) files. Hard-copy versions are available for purchase by contacting the Survey at:

Kentucky Geological Survey
Publication Sales Office
228 Mining and Mineral Resources Building
University of Kentucky
Lexington, Kentucky 40506-0107

Phone: 606-257-5500
Fax: 606-257-1147

Selected KGS reports published before 1999 have been scanned and converted to PDF format. Scanned documents may not retain the formatting of the original publication. In addition, color may have been added to some documents to clarify illustrations; in these cases, the color does not appear in the original printed copy of the publication. Every effort has been made to ensure the integrity of the text. KGS maps and charts are supplied either whole or in part and some are too large to be printed on most plotters. Open-file reports are reproduced from the best available copy provided by the author, and have not undergone KGS technical or editorial review.

The Kentucky Geological Survey disclaims all warranties, representations, or endorsements, expressed or implied, with regard to the information accessed from, or via, this server or the Internet.

UNIVERSITY OF KENTUCKY

Dr. Charles T. Wethington, Jr., President
Dr. Fitzgerald Bramwell, Vice President for Research and Graduate Studies
Jack Supplee, Director, Administrative Affairs, Research and Graduate Studies

KENTUCKY GEOLOGICAL SURVEY ADVISORY BOARD

Kenneth Gibson, Chairman, Madisonville
William W. Bowdy, Fort Thomas
Steve Cawood, Pineville
Larry R. Finley, Henderson
Hugh B. Gabbard, Richmond
Ron D. Gilkerson, Lexington
Dr. Wallace W. Hagan, Lexington
Phil M. Miles, Lexington
W.A. Mossbarger, Lexington
Henry A. Spalding, Hazard
Jacqueline Swigart, Louisville
David A. Zegeer, Lexington
Ralph N. Thomas, Emeritus Member, Owensboro
George H. Warren, Jr., Emeritus Member, Owensboro

KENTUCKY GEOLOGICAL SURVEY

Dr. Donald C. Haney, State Geologist and Director
Dr. John D. Kiefer, Assistant State Geologist for Administration
Dr. James C. Cobb, Assistant State Geologist for Research

ADMINISTRATIVE DIVISION

Personnel and Finance Section:
James L. Hamilton, Administrative Staff Officer II
Jackie Perrelli, Administrative Staff Officer

Clerical Section:
Jody L. Cruse, Staff Assistant VII
Kimberly B. Stroth, Staff Assistant VI
Juanita G. Smith, Staff Assistant V, Henderson Office

Office of Communications and Technology Transfer:
Dr. Carol L. Ruthven, Geologist V, Manager
Margaret Luther Smath, Geologic Editor III
Terry D. Hounshell, Chief Cartographic Illustrator
Michael L. Murphy, Principal Drafting Technician
Gwenda K. Rulo, Drafting Technician
Shirley D. Dawson, Staff Assistant V

Well Sample and Core Repository:
Patrick J. Gooding, Geologist IV, Manager
Robert R. Daniel, Laboratory Technician B

Office of Geologic Information:
Bart Davidson, Geologist IV, Manager
Richard A. Smath, Geologist III, ESIC Coordinator
Kevin J. Wente, Geological Technician
William A. Briscoe III, Publication Sales Supervisor
Roger S. Banks, Account Clerk V
Luanne Davis, Staff Assistant IV
Theola L. Evans, Staff Assistant IV

Computer and Laboratory Services Section:
Steven J. Cordiviola, Head
Richard E. Sergeant, Geologist V
Joseph B. Dixon, Systems Programmer
James M. McElhone, Senior Systems Analyst Programmer
Henry E. Francis, Associate Scientist
Karen Cisler, Senior Research Analyst
Janet M. Royer, Senior Research Analyst
Steven R. Mock, Research Analyst
Alice T. Schelling, Research Analyst
Mark F. Thompson, Research Analyst
Lisa A. Miles, Principal Laboratory Technician
Christopher L. Parsons, Senior Laboratory Technician
Mary C. Koewler, Senior Laboratory Technician

GEOLOGICAL DIVISION

Coal and Minerals Section:
Dr. Donald R. Chesnut, Jr., Head
Dr. Garland R. Dever, Jr., Geologist VII
Dr. Cortland F. Eble, Geologist V
Dr. Gerald A. Weisenfluh, Geologist V
David A. Williams, Geologist V, Henderson Office
Dr. Stephen F. Greb, Geologist IV
William M. Andrews, Jr., Geologist I
Ernest E. Thacker, Geologist I

Geologic Mapping and Hydrocarbon Resources Section:
Dr. James A. Drahovzal, Head
Warren H. Anderson, Geologist V
David C. Harris, Geologist IV
Brandon C. Nuttall, Geologist IV
Lance G. Morris, Geologist II
Thomas N. Sparks, Geologist I
Anna E. Watson, Geologist I

Water Resources Section:
Dr. James S. Dinger, Head
Dr. Daniel I. Carey, Hydrologist V
James C. Currens, Geologist V
Dr. David R. Wunsch, Geologist IV
Philip G. Conrad, Geologist III
R. Stephen Fisher, Hydrologist III
Alex W. Fogle, Hydrologist III
Robert E. Andrews, Geologist II
C. Douglas R. Graham, Geologist II
Timothy D. Montowski, Geological Technician
Gregory L. Secrist, Geological Technician
D. Ian Thomas, Geological Technician
Steven E. Webb, Geological Technician
Kathleen J. O'Leary, Program Coordinator
Wendy S. Romain, Program Coordinator

CONTENTS

ILLUSTRATIONS

ILLUSTRATIONS (CONTINUED)

Figure **Page**

TABLES

Table **Page**

Mission Statement

The Kentucky Geological Survey at the University of Kentucky is a State-mandated organization whose mission is the collection, preservation, and dissemination of information about mineral and water resources and the geology of the Commonwealth. KGS has conducted research on the geology and mineral resources of Kentucky for more than 150 years, and has developed extensive public databases for oil and natural gas, coal, water, and industrial minerals that are used by thousands of citizens each year. The Survey's efforts have resulted in topographic and geologic map coverage for Kentucky that has not been matched by any other state in the Nation.

One of the major goals of the Kentucky Geological Survey is to make the results of basic and applied research easily accessible to the public. This is accomplished through the publication of both technical and non-technical reports and maps, as well as providing information through open-file reports and public databases.

HYDROGEOLOGY, HYDROGEOCHEMISTRY, AND SPOIL SETTLEMENT AT A LARGE MINE-SPOIL AREA IN EASTERN KENTUCKY: STAR FIRE TRACT

David R. Wunsch, James S. Dinger, Page B. Taylor, Daniel I. Carey, and C. Douglas R. Graham

ABSTRACT

An applied research program at the Star Fire surface mine in eastern Kentucky, owned and operated by Cypress-AMAX Coal Co., defined spoil characteristics to develop and monitor water resources, which will help identify a reliable water supply for future property development. Water stored in the mine spoil may provide a usable ground-water supply, and the spoil could also be engineered to provide base flow to surface-water reservoirs.

Ground-water recharge enters the spoil by way of sinking streams, ground-water flow from bedrock in contact with the mine spoil, and a specially designed infiltration basin. Ground water discharges predominantly from springs and seeps along the northwestern outslope of the spoil.

A conceptual model of ground-water flow, based on data from monitoring wells, discharge from springs and ponds, dye tracing, hydraulic gradients, and field reconnaissance, indicates that ground water moves slowly in the spoil interior, where it must flow down into the valley fills before discharging out of the spoil. Two saturated zones have been established: the first in the spoil interior, and the second in the valley fills that surround the main spoil body at lower elevations. The saturated zone in the valley fills contains fresher water than the zone in the spoil interior and exhibits more water-level fluctuation because of efficient recharge pathways along the spoil's periphery at the spoil-highwall contact. The average saturated thickness of the valley fill areas (30.1 ft) is approximately twice the average saturated thickness found in the spoil's interior (15.4 ft). Spatial water-quality variations are consistent with those predicted in the proposed flow system.

Based on an estimated average saturated thickness of 21 ft for the entire site, the saturated spoil stores 4,200 acre-ft (1.4 billion gallons) of water. Hydraulic-conductivity (K) values derived from slug tests range from 2.0×10^{-6} to more than 2.9×10^{-5} ft/sec, and are consistent with hydraulic-conductivity data for other spoil areas where similar mining methods are used.

Water samples taken from wells and springs indicate that the ground water is a calcium-magnesium-sulfate type, differing mainly in the total concentration of these constituents at various locations. Mineral saturation indices calculated using the geochemical model PHREEQE indicate that most of the ground water is near equilibrium with gypsum. Nearly all the water samples had pH measurements in a favorable range between 6.0 and 7.0, indicating that the spoil does not produce highly acidic water.

Measurements of vertical displacement around the monitoring-well surface casings indicate that differential settlement is occurring within the mine spoil. The most rapid settlement occurs in the most recently placed spoil near the active mining pit.

INTRODUCTION

Even though Kentucky's high coal production rates have remained steady, the mining-related work force has been reduced approximately 33 percent since 1980. General unemployment in both coal-mining areas is estimated to be 25 percent because of the lack of economic development except for mining. Economic diversification in eastern Kentucky is hampered by the lack of water supplies and flat usable land. Although significant areas of relatively flat land are continuously being created by surface-mining operations throughout this area, the availability of water resources to sustain industrial development or agriculture remains questionable.

This study evaluates the potential development of water resources in a thick and extensive spoil at the reclaimed site to (1) define the hydrogeology of the site, leading to the definition of the flow system, (2) characterize the ground-water geochemistry to create baseline data for long-term monitor-

ing, (3) delineate temporal and spatial variation in water chemistry, and (4) make a preliminary evaluation of spoil settlement to determine its constraints on future development. This study will contribute to the basic understanding of the hydrogeology and hydrogeochemistry of large spoil areas and result in baseline data and technology that may be applicable to other reclaimed mine areas in eastern Kentucky and the Appalachian coal field.

Geologic and Hydrogeologic Setting

The Star Fire Mine encompasses parts of Breathitt, Perry, and Knott Counties and is located approximately 5 miles northeast of Hazard, Ky., off the Daniel Boone Parkway (Ky. Highway 80) (Fig. 1). Regional geology of the site is mapped on the Noble (Hinrichs, 1978) and Vest (Danilchik and Waldrop, 1978) 7.5-minute geologic quadrangle maps. Figure 2 is a generalized geologic column for the mine site. The coals being mined include the Hazard Nos. 7, 8, 9, and 10, all of which are part of the Breathitt Formation of Pennsylvanian age. These coals are high-volatile bituminous and range in thickness from 3 to 7 ft. Several zones contain rider coals, thin coal beds adjacent to the major beds, which are also mined. The overburden consists of interbedded sandstones, shales, siltstones, and underclays. Some units are locally calcareous, or may contain lenticular calcareous concretions (Spengler, 1977). In the process of mining, backfill (spoil) up to 300 ft thick is being created.

Weinheimer (1983) studied sandstone samples from four cores representing the Breathitt Formation at a site approximately 3 miles from the mine. Analyses revealed the following average component percentages (thus, the sum of the components does not equal 100 percent): quartz, 47.0 percent; feldspar (mainly potassium feldspar), 29.0 percent; rock fragments, 11.9 percent; mica, 5.4 percent; and heavy minerals (pyrite, siderite), 0.5 percent. The majority of the cement was determined to be ferroan calcite. Abundant authigenic kaolinite filled pore spaces and formed reaction rims around feldspar grains. The occurrence of dolomite in Breathitt rocks is rare. Shales and claystones in the Breathitt Formation contain illite, kaolinite, and chlorite (Papp, 1976).

Analyses performed to obtain the initial mining permit (Soil and Material Engineers, Inc., 1982) predicted that the overburden should not produce acid-mine drainage problems because of the high net neutralization potential. The high neutralization potential was attributed to the abundance of carbonate cements in the overburden sandstones. All pre-mining overburden analyses show a potential acidity (PA) of less than 5. PA is the acidity, expressed as equivalents of calcium carbonate ($CaCO_3$), calculated from pyritic sulfur content. If PA is less than 5, the stratum is generally considered a non-acid producer, regardless of the neutralization potential (Sobek and others, 1978).

Ground water is stored in the unmined bedrock that surrounds the mine. The dominant pathways for ground-water movement are coal seams, and near-surface and regional fracture systems (Kipp and Dinger, 1991; Wunsch, 1992).

Ground-Water Considerations

Aquifer Framework

Discussions with mine personnel and direct observation of the mining process demonstrated that selected spoil-handling techniques have produced a rock framework conducive to the development of an aquifer within the spoil. Several

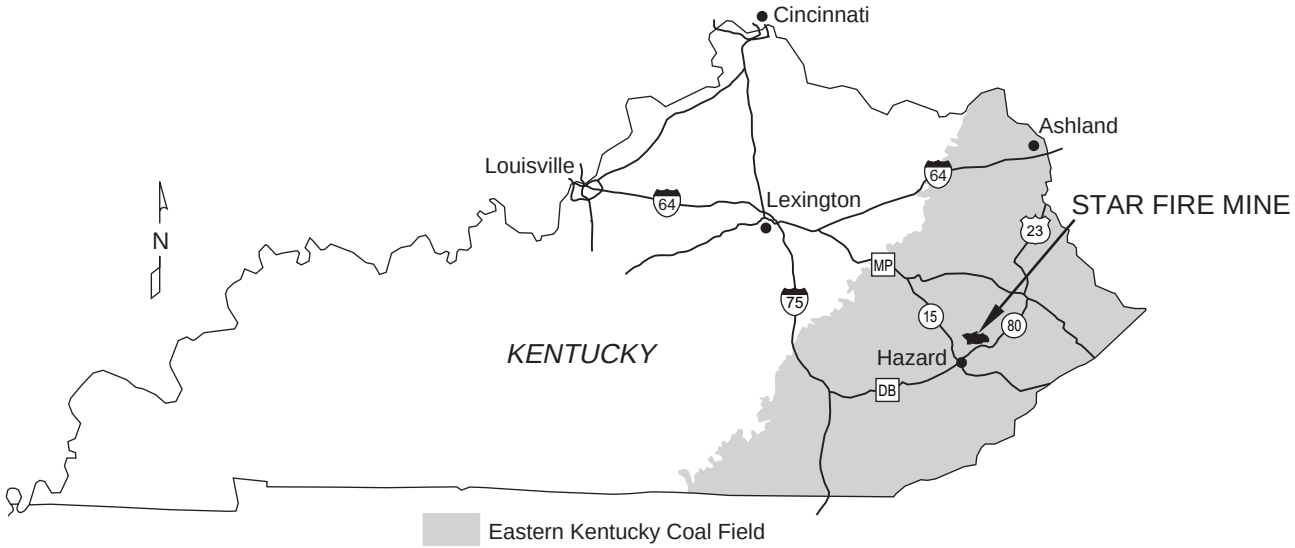

Figure 1. Location of the Star Fire Mine. DB=Daniel Boone Parkway. MP=Mountain Parkway.

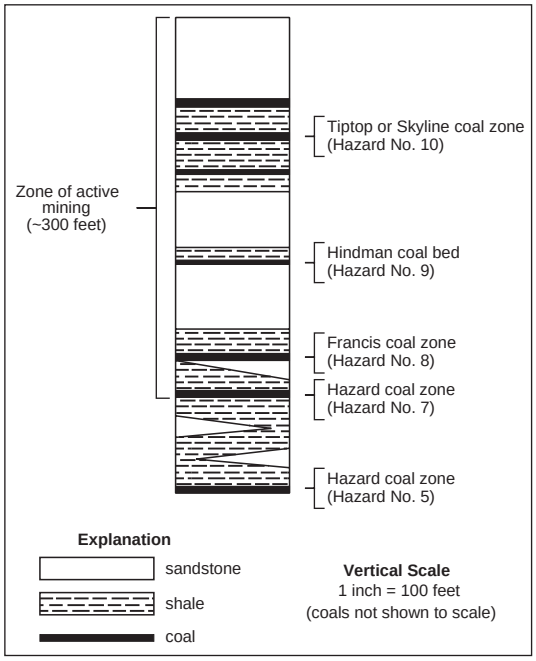

Figure 2. Schematic geologic column showing near-surface coals in the study area. All units are part of the Breathitt Formation of Pennsylvanian age. Modified from Kemp (1990).

previous papers have described, in detail, blasting effects, gravity settling and sorting, selective dumping, and compaction of the spoil and the implications of these factors in controlling the movement and storage of ground water at the site (Dinger and others, 1988, 1990; Wunsch and others, 1992). Therefore, these factors will be discussed only briefly here.

Figure 3 illustrates the transformation from the pre-mining bedrock topography to the landscape resulting from the extraction of the Hazard Nos. 7, 8, and 9 coal beds. Overburden is removed by alternating episodes of cast blasting and spoil removal by a 64-cubic-yard bucket dragline (cast blasting is a process in which explosives are placed in holes drilled along the highwall, and the rock is directionally blasted and "cast" into the bottom of the pit; large, boulder-size chunks of rock typically accumulate at the bottom of the spoil as a result). The lowest coal being mined is the Hazard No. 7. The shale bedrock remaining in place after the removal of the coal creates a pavement that forms a relatively impermeable lower boundary for any water that accumulates in the spoil. Figure 3b shows the continuous, coarse boulder zone created by cast blasting the adjoining bedrock. Spoil covering the boulder layer is placed by the dragline, electric shovels, and dumping of large rocks by dump trucks (Kemp, 1990).

Figure 4 is a detailed cross section of the spoil; it illustrates the spoil structure in which various mining methods and spoil placements are being used. Unmined valleys are sometimes filled with durable boulders, creating a zone of higher hydraulic conductivity, which provides subsurface drainage for the mine (Fig. 4, feature A). The continuous coarse boulder zone on top of the unmined bedrock (Fig. 4, feature B) ranges from 15 to approximately 30 ft in thickness and usually consists of the underburden of the Hazard No. 9 coal. This spoil is cast-blasted into the open pit after the No. 7 coal is removed. This zone, and similar boulder zones found in valley fills, should permit the storage and rapid movement of ground water. Because of their thick and continuous nature, and their position on the bedrock floor, these zones should be the most capable of providing and storing significant amounts of ground water.

The spoil material cast by the dragline produces numerous inclined layers of coarse aggregate above the boulder zone (see Fig. 4, feature C). These layers are created by gravity sorting of the spoil material when it is dumped from the dragline bucket: the larger, heavier rock fragments separate from the finer material and accumulate from the bottom up along the outer edge of each spoil cone. As mining continues, the spoil cones and therefore the coarse layers coalesce to create interconnected pathways for ground-water movement. These pathways may act as recharge routes from the land surface to the boulder zone at the base of the fill, and the finer material at the base of the spoil cones may behave as an extensive storage reservoir for ground water as the spoil becomes saturated.

Another sequence of coarse inclined layers is also found in the upper part of the spoil material, where spoil has been dumped by trucks (Fig. 4, feature F). The coarse rock layers are similar to the cast-dragline spoil, but are not as thick or as extensive.

In contrast to the coarse permeable zones, relatively impermeable compacted zones are also produced by mining within and on top of the spoil (see Fig. 4, features D, E, and G). The final compacted graded land surface (see Fig. 4, feature G) can inhibit surface water from infiltrating into the spoil material. Therefore, special spoil-handling techniques have been used to capture surface runoff for recharge to the ground-water system within the spoil material.

Infiltration Basin Design and Construction

An infiltration basin was constructed that would create a direct connection to the rubble zone resting on top of the No. 7 coal underburden (Fig. 4), and would lead to an understanding of water movement and recharge potential of the spoil after the infiltration basin was operational. An extensive rock drain consisting of sandstone boulders was created to bypass all intermediate compacted zones within the spoil that might tend to perch percolating ground water (see Fig. 4).

Directing surface runoff into the infiltration basin can have an additional benefit. Typically, surface-water runoff flowing from large spoil areas contains high amounts of suspended

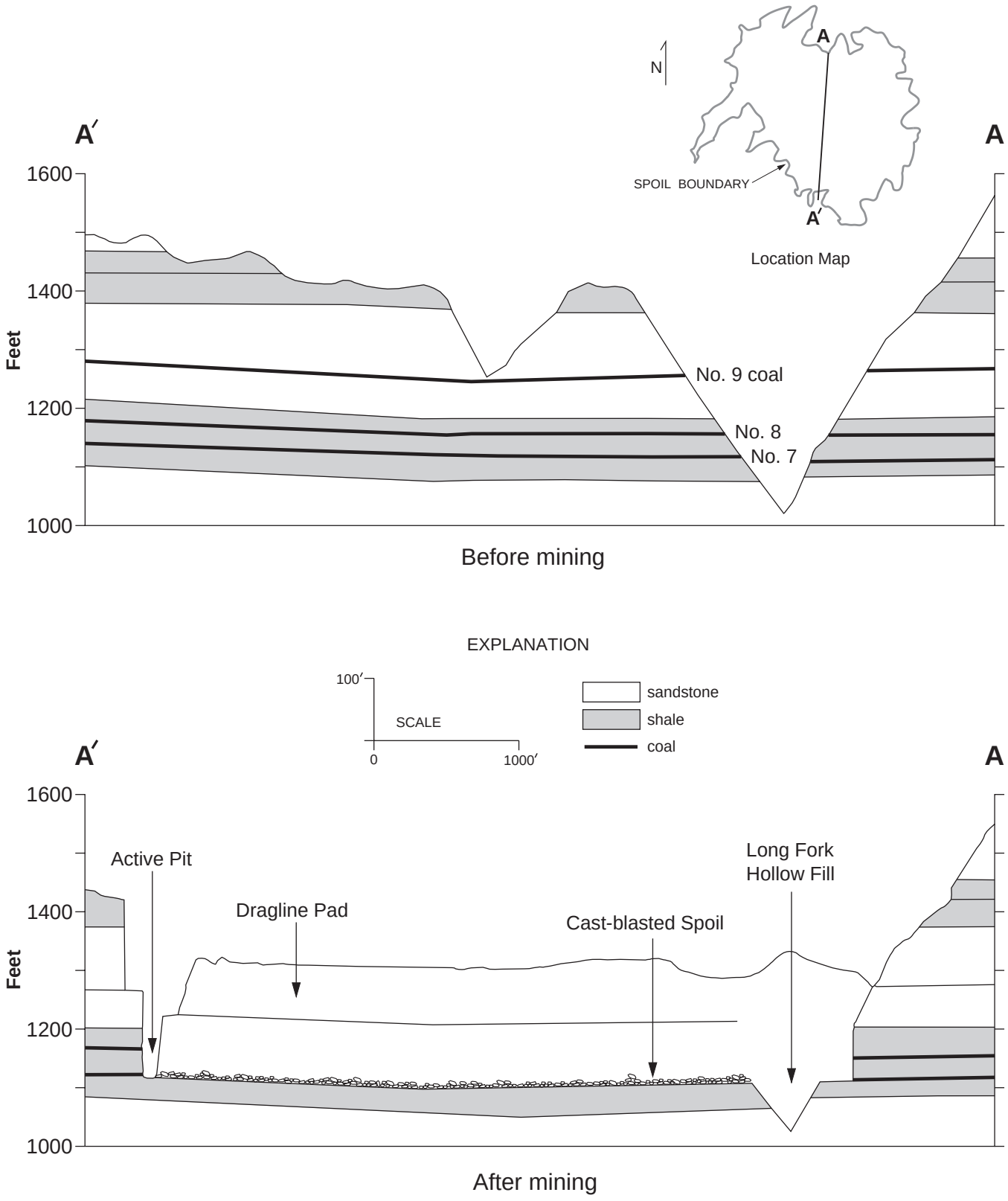

Figure 3. Before- and after-mining cross sections. Inset shows location of cross sections. Modified from Kemp (1990).

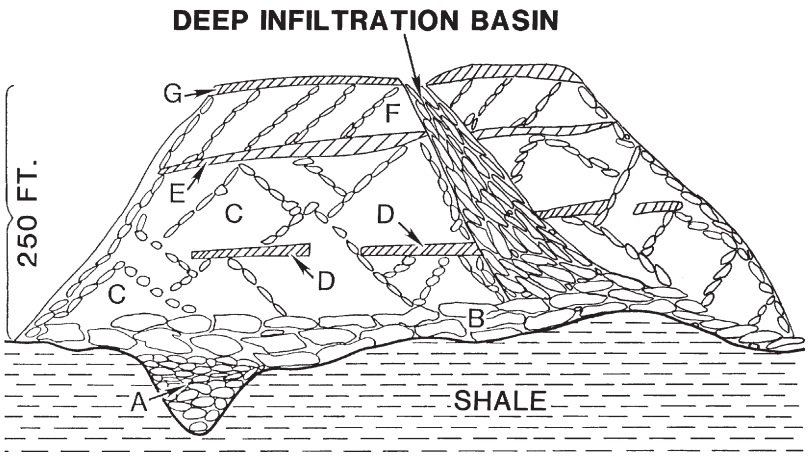

Figure 4. Schematic cross section showing components of spoil significant to the development of an aquifer framework. A=hollow fill. B=cast-blasted rubble. C=dragline spoil. D=dragline pad. E=temporary haul road. F=truck-dumped spoil. G=final graded land surface.

solids and sediment, which leads to sedimentation problems in nearby streams. Surface water directed into the infiltration basin is filtered by the porous media as it percolates down to the saturated zone. Introducing artificial recharge through the infiltration basin may help minimize sedimentation problems in streams surrounding the mine site. Sediment will most likely still have to be removed from the bottom of the infiltration basin, however.

Water Monitoring Methods

Methods used to characterize the hydrogeology of the spoil include precipitation measurements, discharge measurements of streams and springs, ground-water dye tracing, water-level measurements from monitoring wells, falling-head slug tests, and water-quality analyses.

Figure 5 shows the locations of a precipitation gage, a discharge flume, monitoring wells, and a stilling well around the periphery of the infiltration basin. The stilling well consists of a pressure transducer to measure water stage installed within a length of PVC well casing that descends to the bottom of the basin. Daily precipitation data have been recorded at the site with a tipping-bucket device equipped with a pulse recorder and data logger. The flume and stilling well measure discharge and stage, respectively, by converting direct head measurements collected by digital data loggers. The digital data loggers record data from pressure transducers.

Surface-Water Flow Measurements

Surface-water flow was measured at recharge and discharge points at the site. Flow measurements were made using a hand-held meter and summing the flow-velocity readings taken at even increments along a cross section of the stream channel. This method yields a maximum accuracy of within 5 percent of actual discharge (U.S. Geological Survey, 1980). The total mine outflow was measured at a flume located below the sediment-pond discharge. The flume was equipped with digital stage recorders, and discharge was determined by establishing a rating curve based on stage levels. Mass balance was calculated to determine missing components of flow, using surface-water flow data and flume measurements.

Monitoring Wells

Monitoring wells were installed to study the establishment and fluctuations of a water table in the spoil, characterize the ground-water quality, determine the effectiveness of the deep infiltration basin, and determine the hydraulic properties of the spoil. Installation of monitoring wells in deep spoil was

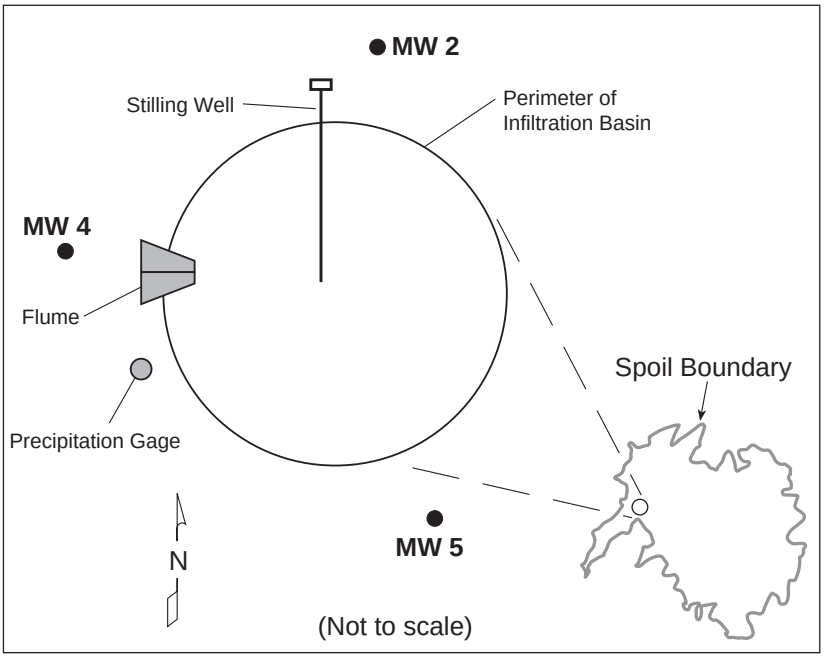

Figure 5. Schematic diagram showing the location of monitoring wells and instruments near the deep infiltration basin.

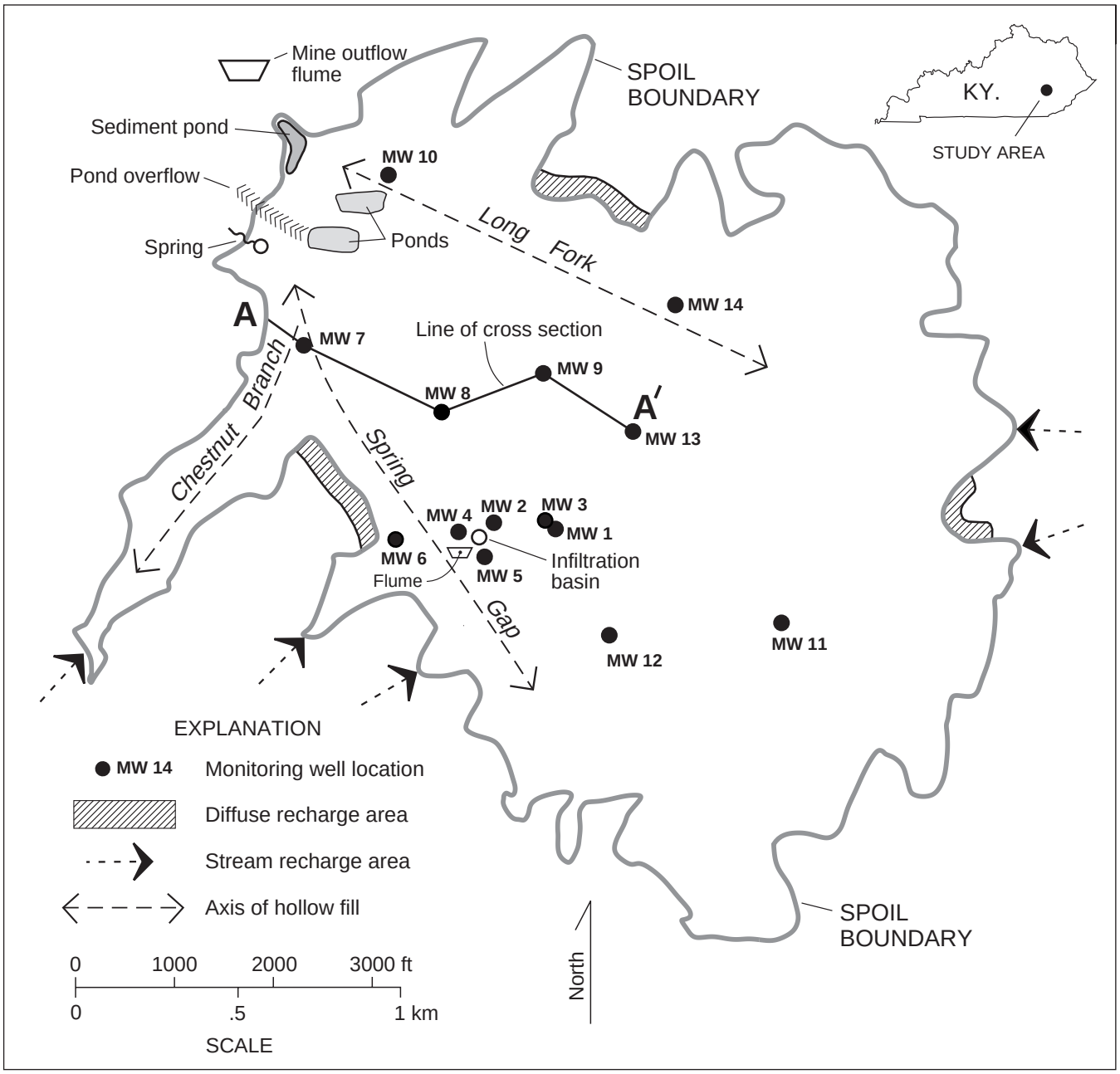

Figure 6. Significant features at the Star Fire site. The southeastern boundary of the mine spoil is approximate because of continuing mining.

hampered by heterogeneity of the spoil, which contains particle sizes ranging from clay to large sandstone boulders; lack of consolidation and spoil instability; and slump and collapse in the saturated zone.

The locations of monitoring wells at the site are shown in Figure 6. Three methods of monitoring-well installation were attempted at the site; each succeeding drilling episode contributed to an ultimately successful design that maintained well integrity in the dynamic subsurface environment of the thick mine spoil. Monitoring well (MW) 1 was drilled using the cable-tool method. Problems with this technology were: unsuccessful attempts to drive steel casing to prevent collapse of the spoil, loss of borehole integrity when the drill bit encountered the saturated zone, and extremely slow drilling rate.

Monitoring wells 2 and 3 were drilled using an air-rotary method, in which a welded steel casing was driven into the spoil behind the advancing drill bit to prevent collapse. This method required pulling the drilling rods out in order to drive in the surface casing and weld on additional sections. Once the casing was installed, the production screen and pipe were

lowered into the hole. A gravel pack was placed around the screen while the steel surface casing was pulled back. Wells 2 and 3 were completed with 4-inch-diameter, flush-joint, schedule-40 PVC pipe. We subsequently discovered that settlement and shifting of the spoil caused failure and rupturing where the plastic casing was unprotected.

The third monitoring well design utilized an air-rotary drilling rig equipped with a pneumatic-hammer, under-reaming drill bit with a hardened steel collar that expands as the hammer rotates below an advancing steel casing. The steel casing was simultaneously driven as the drill bit advanced. The protective casing was left in the hole for increased well integrity after an initial pullback to expose the well screen and install the gravel pack. Two-inch-diameter, schedule-40 stainless-steel screens were attached to schedule-40 PVC production pipe, creating a "hybrid" monitoring well (Fig. 7). The PVC pipe was encased within the steel protective casing; thus, all external monitoring-well materials in contact with spoil material were made of steel. The annular space between the steel protective casing and the PVC pipe was filled with bentonite, which allowed for slight plastic deformation of the production pipe as a result of spoil settlement and adjustment.

A total of 11 monitoring wells (wells 4 through 14), ranging in depth from 54.7 to 239.0 ft, were installed as illustrated in Figure 7, using the under-reaming bit. Various monitoring wells were equipped with continuous data loggers to record changes in the water table for extended periods of time.

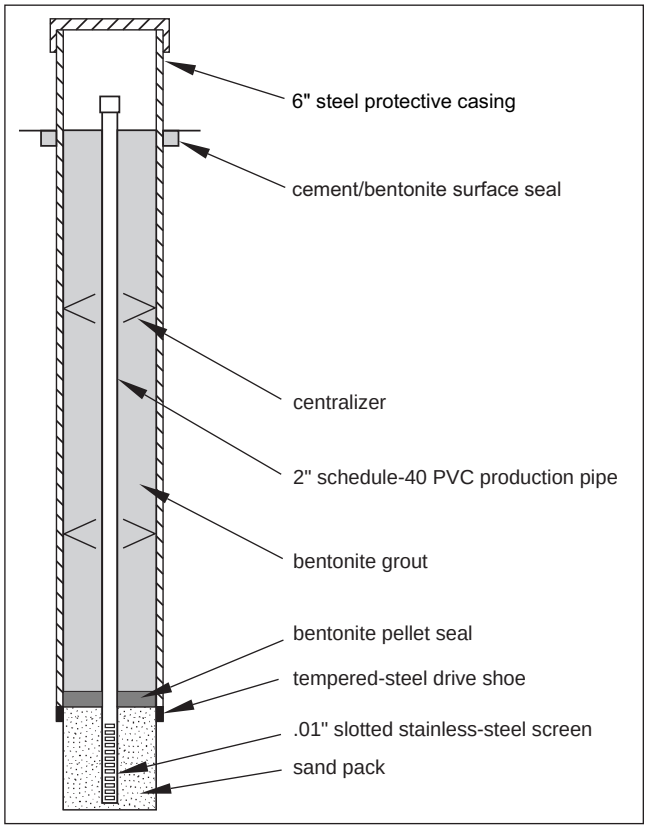

Figure 7. Design for monitoring wells 4 through 14. Drawing not to scale.

Slug Tests

Falling-head slug tests determined the spatial distribution of hydraulic conductivity and the range of variability within the spoil. Nine tests were performed by injecting ground water derived from the spoil as quickly as possible into the monitoring wells until the water level reached the top of the plastic casing. Usually, the well casing was filled with water in less than a minute. An equilibrium water level was maintained while any trapped air bubbles were allowed to escape from the water column. The instantaneous drop in head when the water flow was cut off was recorded by a submerged pressure transducer that stored the head data on a digital data logger. This technique is based on methods first described by Hvorslev (1951) in the development of "time-lag" permeability tests. Hvorslev's method assumes that instantaneous changes in water level occur at the initiation of a slug test, which was not the case in this study. Even under ideal conditions, Hvorslev's method is not precise. However, it is generally considered an appropriate means of estimating the order of magnitude of hydraulic conductivity (Thompson, 1987).

Hydraulic-conductivity values were calculated using the computer program TIMELAG (Thompson, 1987). This program contains several cases that are employed depending on the well-configuration data provided. Unconfined aquifer conditions were assumed.

In some cases, wells took more water than could be injected by the pump (50 gallons per minute [gpm]). In these wells, the hydraulic conductivity calculated represents a minimum value based on a water-injection rate of 50 gpm. The static head level used for calculations was the maximum head level (top of casing) for each well, which provided for a minimum hydraulic conductivity value that would sustain the maximum flow rate. Actual hydraulic conductivity values must be higher than these calculated values.

Water-Quality Sampling and Analysis

Samples were collected to determine the chemical character of the surface and ground water at the site, provide input data for geochemical models and mass-balance studies, and establish baseline data in order to monitor temporal and spatial variability in water quality. Samples were drawn and analyzed from the largest spoil spring, monitoring wells, the stream in Chestnut Gap Branch (see Fig. 6), and the deep infiltration basin. All wells were sampled quarterly beginning in the spring of 1991; this sampling scheme will continue as funding permits. Some samples were taken from springs and streams to study recharge events. Field parameters determined for most samples were temperature, specific

electrical conductance, oxidation-reduction potential (Eh), and pH in accordance with U.S. Geological Survey (1980) guidelines for sampling and collecting. Data were collected utilizing a flow-through cell that was closed to the atmosphere. Under these conditions, Eh measurements and subsequent qualitative interpretations of the redox conditions in natural waters could be made (Langmuir, 1971; Champ and others, 1979). Water flow to the cell was provided by a 2-inch-diameter submersible pump, which was used for purging and sampling of the monitoring wells. Laboratory analysis of water samples determined 30 total and dissolved metal concentrations and major anions.

Dye Tracing

Ground-water dye traces defined flow paths and travel times through the spoil. Dye-trace data from previous studies (Kemp, 1990) were also used to define ground-water flow paths in the Spring Gap drainage area. The dye used for all tracing was Rhodamine WT, a fluorescent dye. It has been widely used in the study of karstic carbonate aquifers, and to a lesser extent in granular aquifers (Aulenbach and others, 1978). Rhodamine WT exhibits many properties favorable for ground-water tracing, including detectability at very low concentrations (parts per billion), low toxicity, a distinct peak-emission wavelength, chemical stability over a wide range of pH values, photochemical and biological stability, and a low rate of adsorption (Smart and Laidlaw, 1977). The most critical of these factors for this study is its low rate of adsorption, because the dye is assumed to flow through an aquifer matrix rich in clays, organic-rich shales, and ferric hydroxide. Ferric hydroxide was found to adsorb significant quantities of Rhodamine WT in an experiment designed to test fluorescent dyes for use in ground-water tracing in underground coal mines (Aldous and Smart, 1987). Therefore, ample amounts of dye were used to allow for dilution and adsorption.

Dye traces determined the flow path of water entering the spoil through the deep infiltration basin, Chestnut Gap Branch (a stream that flows into the base of the spoil), and MW 1, which is located in the central area of the spoil (Fig. 6). The flow path of ground water injected with dye at these locations was determined by placing dye detectors, which consisted of permeable textile sacks filled with activated charcoal, at various points of discharge. The elutriant, or solution used to desorb dye from the charcoal detectors, was analyzed with a Turner model 10 filter fluorometer[1].

Spoil-Settlement Measurements

Spoil visibly settled around the monitoring wells that were installed in July 1990. There was vertical displacement between the cement surface seal placed during monitoring-well construction and the surface of the spoil. The spoil was not monitored immediately after the well's emplacement; therefore, settlement could only be assessed for the period after well installation. The displacement between the cement seal and the spoil surface were calculated for each well by making baseline measurements in the four compass directions around the seal of each well. The settlement values were then measured in each direction, and an average value from the four measurements was calculated to represent the spoil settlement at each well. Figure 8 shows an example of surface settlement at MW 4.

Results and Discussion

Recharge Observations

Field reconnaissance of the study area revealed numerous places where streams and storm runoff recharge the spoil aquifer. Recharge at most of these sites is sporadic and often difficult to quantify.

Several streams flow directly into the spoil at the base. The largest is Chestnut Gap Branch, a first-order stream with a watershed area of 0.32 mi^2 (see Fig. 6). Data from Kemp (1990) show that Chestnut Gap Branch had an average flow rate of 0.73 cubic feet per second (cfs) during a 3-month period in 1989, which equates to a 0.47 million gallons per day (mgd) contribution to the total water moving through the spoil.

Recharge from bedrock aquifers occurs where mine highwalls are in contact with the spoil. Although primary permeability is relatively low in the non-coal bedrock forming the highwall (Wunsch, 1992), near-surface and tectonically induced fractures provide highly permeable zones that discharge ground water into the spoil (Kipp and Dinger, 1991).

In some cases, spoil handling resulted in boulders being randomly exposed at the surface. Small (less than 5 cm in diameter), discrete infiltration points, or "snakeholes," were observed where boulders intersect the spoil surface. Storm runoff flows into these discrete holes and rapidly disappears into the spoil. The amount of water that may ultimately reach the saturated zone at the bottom of the spoil by way of these discrete points has not been determined, but is assumed to be minimal compared to the amount of water entering the spoil along the edges of the main spoil body.

Aside from the few discrete infiltration points just described, infiltration through the spoil surface does not account for a significant amount of recharge because of the compacted nature of the graded spoil. Drilling and excavation have shown that the spoil is dry within a few inches of the surface, and a thin sheet of mud quickly forms on the surface after a storm, which indicates that rainfall does not easily infiltrate the spoil. Limited data from a single percolation test performed in the

[1]The use of brand names in this report is for information purposes only, and does not constitute an endorsement.

July 1990

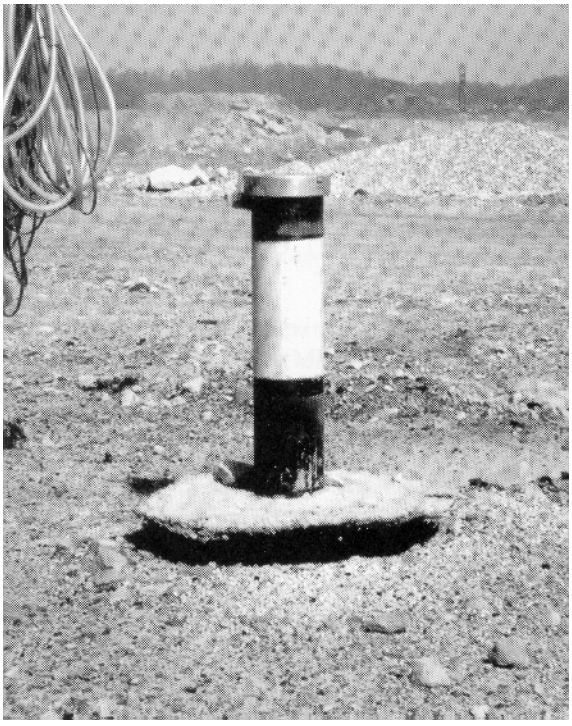

July 1992

Figure 8. Settlement of the mine-spoil surface, as indicated by the movement of the cement surface seals.

vicinity of MW 4 support this observation. The data reveal a very low infiltration rate (0.186 inch/hour) for water entering the spoil through the graded, compacted surface.

On a larger scale, the infiltration basin provides a point source for ground-water recharge. At the present time, the watershed that supplies the basin is limited, and probably contributes relatively insignificant quantities of water in relation to the total amount stored in the spoil. The present watershed surrounding the basin encompasses approximately 18 acres, less than 2 percent of the total spoil area.

Recharge also occurs when precipitation falls directly on ungraded dragline-cast spoil cones or other recently excavated areas. We assumed the infiltration rate in these areas was higher than the rate in the compacted spoil, but have not determined quantitative recharge rates. The size of this spoil cone area varies depending on the amount of grading that has occurred, but is extensive, often 2 million ft^2 or larger (Dinger and others, 1988).

Spring Discharge

The most significant area of discharge from the spoil is in the northwest corner, where a group of three springs is located at the toe of the Spring Gap Branch valley fill (Fig. 6). The springs appear at an elevation of approximately 1,040 ft. The discharge point for the largest of the springs (spring 1) is located at the toe of a 130-ft-thick truck-dumped sandstone spoil that overrides a 45-ft-thick truck-dumped shale spoil. The shale spoil is purported to have a lower permeability than the sandstone spoil (Kemp, 1990). During times of extremely high discharge, a number of small springs have been observed along the toe of this lift at an elevation equivalent to or slightly higher than the main spring. Total discharge from the springs ranges from approximately 1 to 5 mgd (Kemp, 1990).

Discharge was not observed from the toe of the Long Fork valley fill. Mine personnel observed ground water discharging directly into the sediment pond at a point below the pond's water level.

Ground water also discharges from the spoil into the active dragline pit when the pit is at the level of the No. 7 coal. At times, ground water has discharged from the spoil into the active pit at a rate high enough to require pumping on a daily basis. On occasion, pumping rates have reached an estimated 360,000 gpd.

Two ponds have been created to store water for dust control. These ponds, whose locations are shown on Figure 6, are at the northwest corner of the spoil, above the springs. The bottom of the northern pond is on the underclay below the Hazard No. 7 coal. The bottom of the southern pond has been excavated to a lower elevation and is completed within the shale unit below the No. 7 coal and the underclay. Both ponds are fed by water from the saturated spoil, as evidenced by the fact that the water level in the northern pond (1,125 ft), which has no overflow, is very similar to the water level ob-

served in the nearest monitoring well not located over a valley fill (1,130 ft in MW 8). This similarity suggests that the pond is a surface expression of the water table. Also, although these ponds are pumped to fill 10,000-gallon water trucks, the water is never depleted, and the ponds do not freeze in the winter, which suggests a ground-water source. Finally, the electrical conductance (2,100 microsiemens) of the water flowing out of the overflow is similar to that of the spoil-fed springs that discharge below it (Kemp, 1990); if the ponds received their water from surface runoff, the conductance values would be much lower because of dilution. Water overflows from the lower pond throughout the year and cascades down the spoil face by way of a riprap-lined drainage channel and contributes to the total mine outflow.

A large-capacity flume below the sediment pond gages the total water outflow (see Fig. 6 for location). Data have not been continuously collected because of periods of freezing and vandalism, but data were collected on 255 days of the 1992 water year. Table 1 shows the discharge data for several months during the 1992 water year. The monthly mean discharge ranges from 3.08 to 6.95 cfs (2.0 to 4.5 mgd). The mean and median discharge are both approximately 4 cfs (2.6 mgd).

Mass-Balance Calculations

Mass balance was calculated to determine what part of the total mine outflow is provided by the spring that drains the Long Fork valley fill. The spring discharges below water level in the sediment pond at the northwest corner of the spoil, making it impossible to take direct flow measurements or collect water samples (Fig. 6). Flow measurements at all other accessible discharge points were made in June 1994 after a relatively dry spell when streams and springs were considered at base flow. The flow components used in the calculations consisted of the Long Fork flume, spring 1 (SP 1), Chestnut Gap Branch, and the dust-control pond's overflow (see Fig. 6). The cumulative flow for all components was determined by the formula:

$$Q_t = Q_{po} + Q_{cb} + (Q_{sp} - Q_{cb}) + Q_{lf}$$

where

Q_t=measured total mine discharge at the Long Fork flume
Q_{po}=measured discharge of the overflow from the dust-control pond
Q_{cb}=measured discharge from Chestnut Gap Branch
Q_{sp}=measured discharge at the Spring Gap spring
Q_{lf}=calculated discharge from the Long Fork spring.

The discharge from Chestnut Gap Branch was subtracted from the discharge from Spring Gap because Kemp (1990) demonstrated by dye tracing that the total streamflow in Chestnut Gap Branch disappears into the base of the Spring Gap valley fill and re-emerges at spring 1. Thus, it contributes to the flow measured at spring 1. The measured discharge for each site, in cfs, is as follows: Q_t=2.23, Q_{po}=0.84, Q_{cb}=0.20, Q_{sp}=0.63. The flow contribution from the Long Fork drainage (Q_{lf}) is therefore 0.76 cfs.

Mass balance for the total dissolved solid (TDS) load was calculated to determine if the mass loads were consistent with the discharge data. We could not collect a representative water sample from the submerged Long Fork spring. However, MW 10, located approximately 800 ft upgradient from the reported spring discharge site, produces water that is probably representative of the water moving through the Long Fork buried valley, which is the source of the water that discharges from the Long Fork spring. In addition, the coefficient of variation for TDS values from MW 10 is 14 percent (Appendix A), which indicates that the data are consistent. We therefore used the TDS value from MW 10 in the mass-balance calculations.

TDS data for the flow components were determined from samples collected in June 1994, except for the sample from MW 10, which was collected in August 1994 (see Appendix A). The mass-balance formula used in the calculation was:

$$Q_t C_t = Q_{po} C_{po} + Q_{cb} C_{cb} + Q_{sp} C_{sp} + Q_{lf} C_{lf}$$

where

C_t=TDS determined for water from the Long Fork flume
C_{po}=TDS of the overflow from the dust-control pond
C_{cb}=TDS of the discharge from Chestnut Gap Branch
C_{sp}=TDS of the discharge at the Spring Gap spring
C_{lf}=TDS of the Long Fork spring.

Table 1. Discharge data from Long Fork flume, water year 1992.

	Oct. 91	Nov. 91	Dec. 91	Jan. 92	Feb. 92	Mar. 92	Apr. 92	Jul. 92	Aug. 92	Sept. 92
No. of Days	30	30	31	31	29	31	7.60	4.18	31	30
Mean	3.08	3.19	6.95	4.40	4.55	5.13	6.93	3.68	3.57	3.33
Minimum	2.58	2.31	0.17	0.00	3.48	3.75	4.79	3.23	2.63	2.75
Maximum	4.94	16.4	45.0	5.84	11.2	10.0	11.8	5.98	30.0	4.71

Average cfs=4.35. No. of days=255.2. Median cfs=4.04. Data recalculated in March 1995 to reflect revised rating table. No data available for May and June 1992 because of vandalism at the site.

TDS for water derived from the Long Fork spring was determined by the formula:

$$C_{lf} = \frac{Q_t C_t - (Q_{po} C_{po} + Q_{cb} C_{cb} + Q_{sp} C_{sp})}{Q_{lf}}$$

The discharge value for SP 1 is 0.43 cfs, which is the measured discharge (0.63 cfs) minus the recharge component supplied from Chestnut Gap Branch (0.20 cfs). Solving for C_{lf} yields a TDS value of 2,082 mg/L. The TDS of the water sample from MW 10 was 2,113, which is in excellent agreement with the calculated value (a difference of less than 1.5 percent). Moreover, the consistency of the mass-balance calculations suggests that the measurements for discharge sites and the calculated discharge for the submerged spring draining the Long Fork valley fill are reasonable. These calculations show that almost all the total mine outflow can be accounted for by a summation of the ground-water discharge sites located in the northwestern area of the main spoil body.

Dye Tracing

Kemp's 1990 dye trace delineated a flow path between where the Chestnut Gap stream disappears into the spoil and spring 1, located at the northwest corner of the spoil (see Fig. 6). Kemp (1990) also determined an apparent velocity ranging from 0.014 to 0.009 ft/sec based on a straight-line travel distance of 2,400 ft and a travel time between 49 and 73 hours. Chestnut Gap Branch contains high levels of suspended sediment after storms, but the consistently clear discharge at spring 1 indicates that sediment in surface water in Chestnut Gap Branch is filtered by flowing through the spoil. This suggests that directing surface runoff from large spoil bodies through the spoil itself could be an effective technology for treating sediment problems in areas where the mineralogy of the overburden does not create significant acid mine-drainage problems.

A second dye trace by Kemp in 1990 injected dye with a 1,000-gallon slug of water into MW 1 (see Fig. 6). This dye was not recovered in the springs in the northwest corner of the spoil. The dye may have flowed northeast into the Long Fork drainage, but there were no adequate discharge points along this flow route to monitor for dye. Dye was still visible in MW 1 several months after it was introduced, indicating that ground-water movement is sluggish in the vicinity of MW 1. The slow movement of ground water in the vicinity of MW 1 and the lack of dye emerging from the springs also suggests that a low-permeability barrier may exist; or, ground-water movement may be very slow between the interior spoil area and the lower elevation valley-fill areas that encompass the Spring Gap, Chestnut Gap, and Long Fork drainage valleys.

Additional dye tracing in the spring of 1991 determined the flow path of recharge that enters the spoil through the infiltration basin. Dye detectors were set at several locations

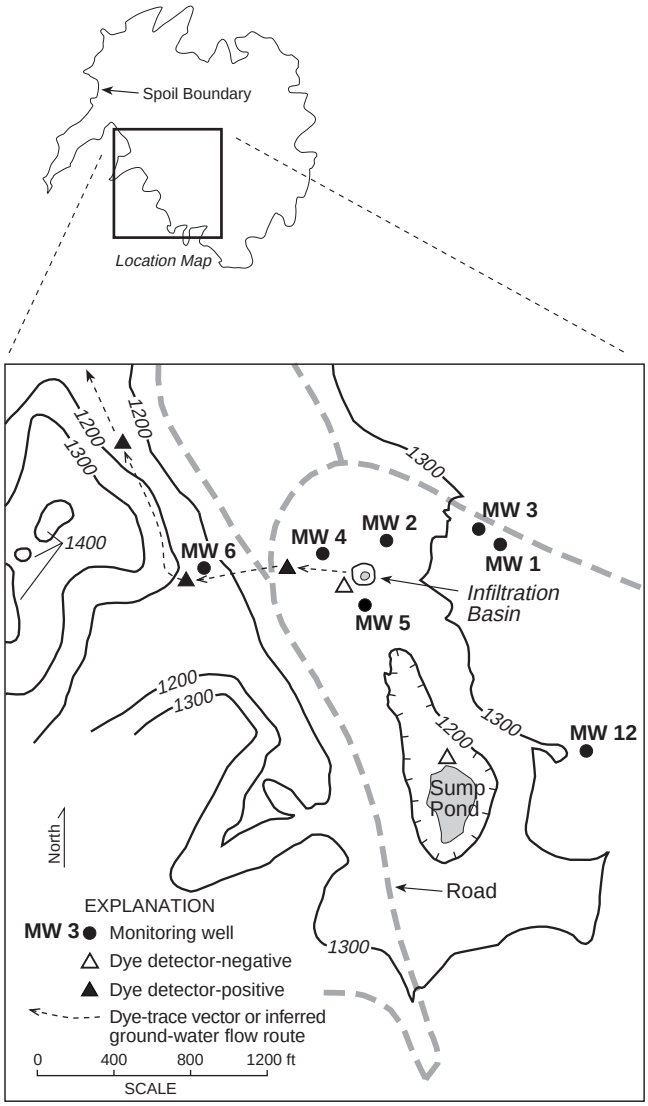

Figure 9. Dye-trace detector locations around the infiltration basin. Contours represent land-surface elevation in ft above sea level.

that were suspected as possible emergence areas for water entering the infiltration basin. Figure 9 shows the locations of the dye detectors. Three positive traces were detected west of the infiltration basin. These results are consistent with the direction of flow indicated by hydraulic gradients and basal topography in this area. One positive trace was also found in a pit excavated along the highwall-valley fill contact near MW 6. Additional positive traces were found where water periodically flowed from the spoil slope between the elevation of the infiltration basin and the valley fill near MW 6. This indicates that not all of the water that flows into the infiltration basin penetrates vertically to the base of the spoil; it may be diverted laterally by low-permeability barriers within the spoil.

The permeability barrier may be created by the spoil-handling techniques that were discussed previously (see Fig. 4), or from sediment clogging the rock chimney (Fig. 4).

Residual dye in MW 1 from Kemp's 1990 dye trace may have contributed to the positive 1991 tests; MW 1 is located near the infiltration basin (see Fig. 6). The infiltration basin is situated between MW 1 and where the positive dye traces were found, however, so movement of ground water is toward MW 6, whether the dye originated from residual dye from the 1990 trace or from the 1991 infiltration-basin test.

Ground-Water Occurrence

Figure 10 shows the outline of the spoil area, along with the contoured surface of the now-buried bedrock topography.

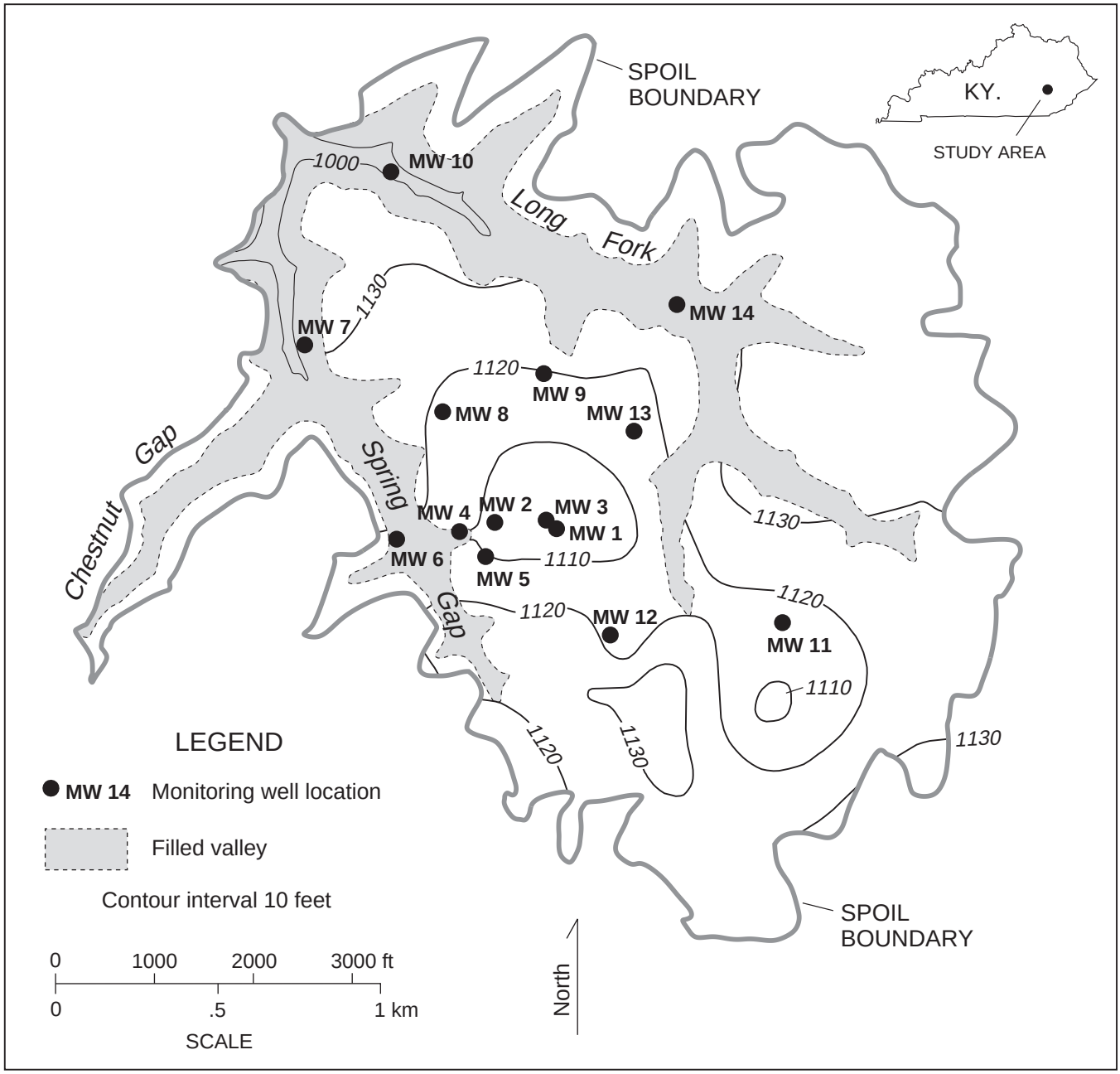

Figure 10. Outline of the spoil and elevation of basal topography.

This map was created by combining the pre-mining topographic map of the mined area and a structure-contour map on the base of the Hazard No. 7 coal, which is the lowest coal being mined. The bottom surface of the spoil's interior is a gently undulating plateau capped by the shale that underlies the No. 7 coal. This buried plateau is bordered by the pre-existing stream drainage (shaded areas on Fig. 10) formed by Long Fork to the northeast and Spring Gap/Chestnut Gap Branch to the southwest. Elevation drops considerably from the plateau level to the bottom of the old stream drainages. Maximum relief (approximately 130 ft) occurs in the northwest corner of the spoil, where the two buried drainage valleys converge around the nose of the plateau.

A contour map of the water table within the spoil (Fig. 11) was created from water-elevation data collected in June 1991 from the 14 monitoring wells on the site, the dust-control pond, and spring 1. There is a slightly mounded water table in the central plateau region, as demonstrated by the closed

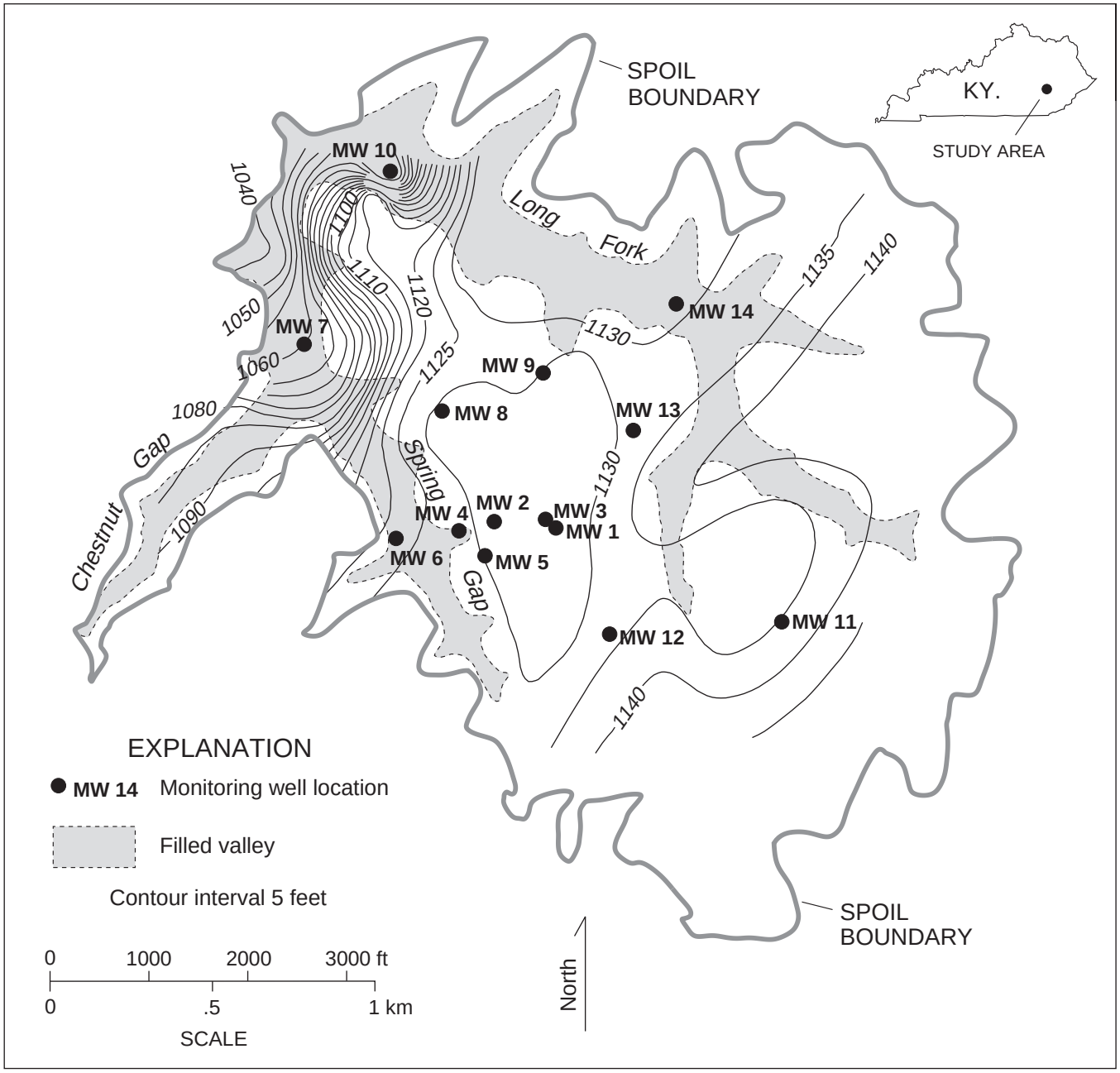

Figure 11. Contour of the spoil water table.

1,300-ft contour line in the center of Figure 11. The water mound is probably a reflection of the spoon-like shape of the mine floor, as shown in Figure 10.

The water-table mound shown in Figure 9 also indicates a low hydraulic gradient in this area. For example, the gradient between MW 9 and MW 13 is 0.0019. The gradient of the water table in the surrounding buried valleys is much higher: the gradient between MW 6 and MW 7 in the Spring Gap valley fill is 0.025, more than 10 times the gradient between the plateau wells.

Steep gradients are also evident between the northwestern area of the plateau and the surrounding buried valleys, which parallel the elevation differences indicated by the buried topography (see Fig. 10). These steep gradients seem unrealistic, and probably represent a boundary between two distinct but interconnected saturated zones.

The distribution of water within the spoil is illustrated in Figure 12, which is a cross section of the spoil through monitoring wells 7, 8, 9, and 13 along line A–A′ (location shown on Fig. 6). There are two saturated zones: one relatively shallow zone perched on the buried plateau, and the other in the valley fill of the Chestnut Gap Branch drainage. The difference in elevation between the buried plateau and the valley bottoms decreases toward the southeast, where the elevation of the valley bottoms gradually rises toward the heads of the valleys. The saturated zones are probably directly connected in the heads of the valleys, where the buried valleys intersect the base of the plateau. The spoon-like shape of the interior basal plateau suggests that the bedrock along the edges of the plateau may form barriers that retard ground-water movement into the valley, where the difference in elevation is greater. This interpretation is supported by the dye-tracing data, which show that water movement is restricted in the interior of the spoil. The water levels in wells on the north side of the spoil suggest a similar configuration in the Long Fork valley fill.

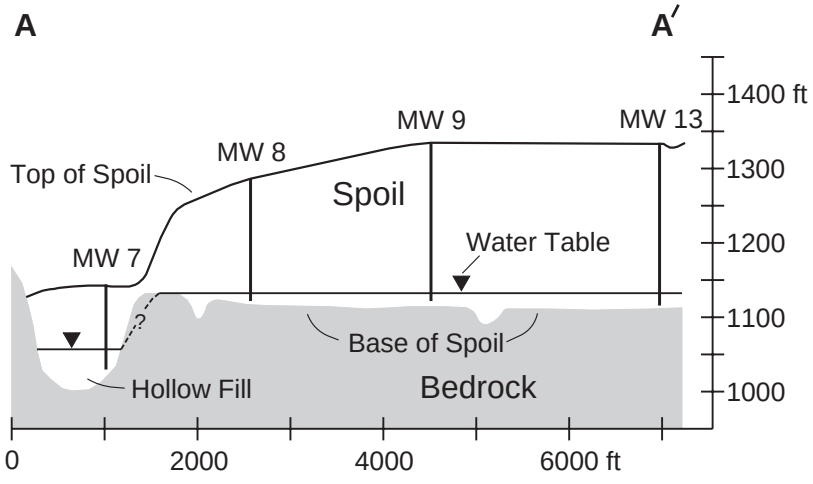

Figure 12. Cross section through line A–A′.

The apparent lack of hydraulic continuity and the low hydraulic gradient in the plateau region suggest that the majority of ground water moving through the spoil flows through the two buried valleys before finally discharging in the northwest corner of the spoil. This conclusion is also supported by the dye-trace data, which show that water moves through the buried valleys at high velocities.

The occurrence of water in each well in the spoil indicates that a significant amount of ground water has accumulated. Table 2 compares the saturated-thickness data for the five wells located in the valley fills with the eight wells located over the spoil's interior (buried plateau). Based on the June 1991 water levels, the mean saturated thickness for the valley-fill wells (30.1 ft) is approximately twice the mean value (15.4 ft) for the wells located over the spoil's interior. The greater saturated thickness in the valley fills may be the result of low-permeability spoil at the mouths of the valleys retarding drainage from the valley fills and allowing for the accumulation of water (Kemp, 1990). In addition, the lower elevation of the valley bottoms, and constriction of flow because of the V shape of the incised, pre-mining valley, compared to the relatively flat bottom of the No. 7 coal underlying the plateau region, may also be factors. The increase in recharge along the edge of the spoil in the valley fills, in contrast to the lack of direct recharge over the main spoil body, may also contribute to the difference in saturated thickness.

Based on an average saturated thickness of 21 ft for all spoil wells, and assuming an estimated porosity of 20 percent, approximately 4,200 acre-ft (1.4 billion gallons) of water is stored within the existing 1,000 acres of reclaimed spoil. Diodato and Parizek (1994) found that the porosity of mine spoil ranged from 30.1 to 57 percent in shallow, unsaturated boreholes, but because of the thick spoil, compaction, and saturated conditions at the Star Fire site, the 20 percent porosity estimate used here seems appropriate.

Hydrographs for the monitoring wells reveal some important facts about the ground-water system. Figure 13 shows the daily water-level averages for monitoring wells 6, 9, and 11. These data were collected using digital data loggers. Water level gradually increased in each well from May 16, 1991, through June 19, 1991. Wells 9 and 11, which are located in the interior of the spoil, exhibited a steady, gradual rise in water level, while MW 6's water levels fluctuated erratically, in a pattern that closely paralleled the precipitation during the observation period. The net rise in water level for MW 6 is similar to the approximately 1 ft increase exhibited by wells 9 and 11 during this period.

MW 6 is located near a bedrock highwall that resulted from contour-cut mining in this area during the 1950's. The rapid response to precipitation in MW 6 is most likely caused by surface

runoff quickly entering the spoil along the contact of the spoil and the bedrock valley wall and by ground water entering the valley fill from the bedrock in contact with the spoil.

Similar responses to precipitation are also seen in the hydrographs for well 7 (Fig. 14) and wells 9 and 14 (Fig. 15) from December 1993. Each well had a net increase in water level during the period. However, the hydrographs for valley-fill wells 7 and 14 indicate that these wells are much more responsive to precipitation than well 9. The increase in water levels following recharge in wells 7 and 14 is probably caused by the same recharge mechanisms described for MW 6.

In summary, the hydrographs for wells 9 and 11 show a relatively smooth response to precipitation, suggesting that the interior of the spoil does not obtain ground-water recharge as readily as the spoil in the valley fills located near the periphery of the spoil (wells 6, 7, and 14). The thickness of the saturated zone in the spoil is a function of the elevation of the bedrock aquitard below the spoil and other barriers to ground-water flow. Generally, the higher the bedrock surface elevation, the thinner the saturated zone. In the valley-fill areas the saturated zone is influenced by the pre-existing surface topography of the unmined areas.

Table 2. Saturated thickness in monitoring wells in June 1991.

Wells Placed Over Hollow Fills			*Spoil-Interior Wells*		
Well ID	*Saturated Thickness*	*Water Elevation*	*Well ID*	*Saturated Thickness*	*Water Elevation*
			2	21.0	1,132.0
			3	10.1	1,131.6
			5	23.1	1,132.4
4	24.5	1,128.4	8	10.6	1,131.1
6	23.7	1,121.6	9	9.5	1,130.4
7	27.1	1,059.5	11	17.6	1,135.3
10	37.1	1,048.8	12	16.7	1,133.1
14	38.0	1,123.0	13	14.7	1,131.5
n=5 range=23.7–38.0 median=27.1 mean=30.1			n=8 range=9.5–23.1 median=15.7 mean=15.4		

Slug Tests

Falling-head slug tests were performed in nine monitoring wells at the site during the fall of 1992. The results of the tests are shown in Table 3. The hydraulic conductivity (K) values ranged from 1.0×10^{-6} to greater than 2.9×10^{-5} ft/sec. These values are comparable to K values for silty sand (Freeze and Cherry, 1979), and are also consistent with hydraulic-conductivity values determined by other studies of mines that use similar mining methods. For example, Oertel and Hood (1983) found K values ranging from 1.5×10^{-6} to 6.9×10^{-4} ft/sec, and Herring and Shanks (1980) found a range from 1.5×10^{-6} to 1.6×10^{-3} ft/sec.

Because some wells (5, 8, 10, and 13) were able to disperse water at a rate that exceeded injection and data-recording capabilities, only a minimum hydraulic conductivity could be calculated. However, judging from the past pumping performance of these wells, and keeping in mind that the flow of water in mine spoil tends to move along discrete high-porosity zones (Caruccio and Geidel, 1984), the actual K values for these wells are probably significantly higher than the values calculated. Because there is no discernible difference in hydraulic conductivity between the wells in the valley fills and wells in the spoil interior, the apparently sluggish ground-water movement in the spoil interior must be related to the low gradients induced by recharge-discharge relationships.

Infiltration Basin

The deep infiltration basin catches surface-water runoff from an 18.9-acre catchment area. The volume of water flowing into the basin for any recorded precipitation event can be calculated by using the stage-discharge curve for runoff that is recorded by the flume and stage recorder. The water level of the pool that accumulates in the basin is recorded by a pressure transducer and digital data recorder in a stilling well (see Fig. 5).

Response of pool levels to precipitation events from May 16 through June 6, 1991, is shown in Figure 16. The response of water entering the basin to a storm is nearly instantaneous, indicating very rapid runoff.

Data from a storm on May 29, 1991, are given in Figure 17. The runoff passing through the flume into the infiltration basin during this event was calculated to be 24,390 ft^3 (182,000 gallons). Three hours passed before all of the water infiltrated into the base of the basin, indicating that the average infiltration rate of the basin was 136 ft^3 (1,010 gallons) per minute.

The percentage of rainfall measured as runoff for the May 29, 1991, storm was 22 percent. Data collected from 42 storms (Appendix B) showed the percentage of runoff varied from a low of 0.82 to a high of 34.3 percent, with an average of 11.9 percent. These data indicate that, on average, 88 percent of precipitation either infiltrates directly into the spoil, is transpired by vegetation, or evaporates directly from the spoil's surface.

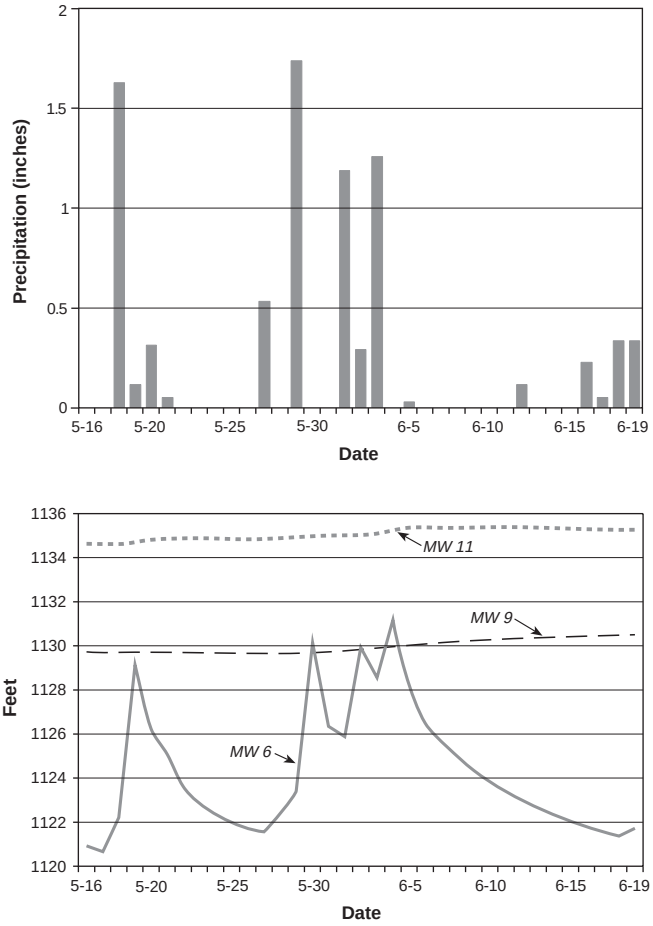

Figure 13. Precipitation and well hydrographs for monitoring wells 6, 9, and 11 from May 16 through June 19, 1991.

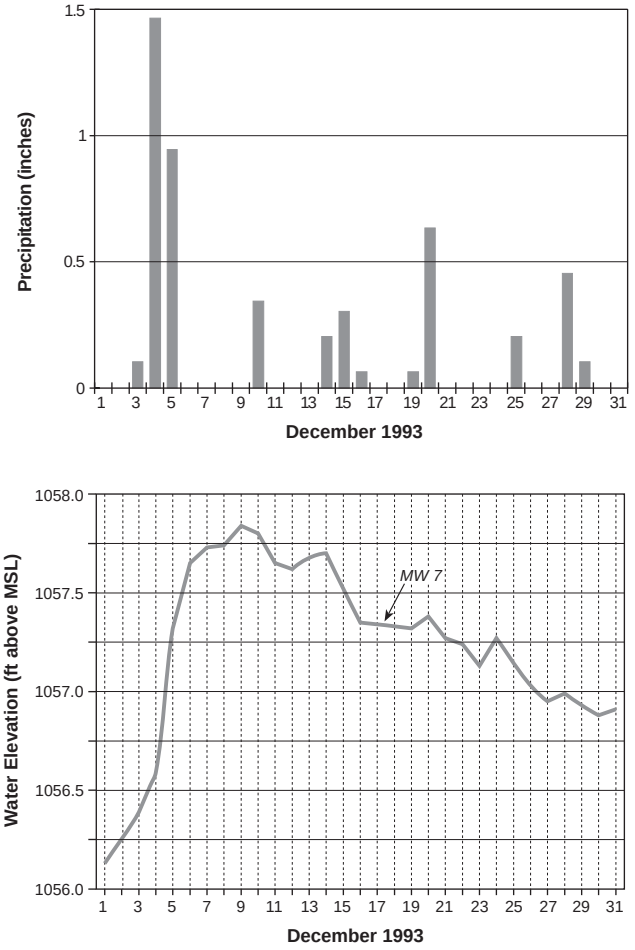

Figure 14. Precipitation and well hydrographs for monitoring well 7 for December 1993.

Typically, the upper few inches of spoil consists of sandstone or siltstone cobbles contained in a sandy, uncemented matrix. This thin zone of spoil is capable of absorbing water at its surface. For example, using the May 29 storm data and assuming no evaporation, 78 percent, or 1.3 of the 1.64 inches resulting from the storm would be available for infiltration into the spoil's surface. Using the lower porosity value for shallow spoil of 30.1 percent determined by Diodato and Parizek (1994), calculations indicate that the upper 4.3 inches of spoil could store all of this water. A thin rind of saturated spoil at the surface would result; this is, in fact, what we observed during excavation immediately after storms (Wunsch and others, 1992).

Three monitoring wells (2, 4, and 5) were placed around the periphery of the basin to monitor the changes in water levels in the spoil as a result of recharge (refer to Fig. 6 for well locations). The water levels for these wells during March, June, and July 1991 are shown in Table 4.

The water level in MW 4 was consistently lower than levels in wells 2 and 5 by nearly 4 ft. The hydraulic gradient implied by these measurements suggests that the water entering the basin flows in the direction of MW 4 (southwest) toward the Spring Gap valley fill. Monitoring well 4 was placed in or near one of the small drainage valleys (shaded in gray on Figure 10) on the upper reaches of the buried Spring Gap stream drainage. The 1,110-ft contour and surrounding intervals indicate a structural low beneath the infiltration basin that opens in the direction of the Spring Gap valley fill. The gradient depicted by the wells surrounding the infiltration basin and also shown by the water-level contours on Figure 11 is consistent with the dye-trace data, which show that the Spring Gap valley fill is capturing the water infiltrating into the spoil through the infiltration basin.

Conceptual Model for Ground-Water Flow in Spoil

Figure 18 is a digital terrain model showing the post-mining bedrock topography buried beneath the spoil and features such as the buried plateau and the Spring Gap and Long Fork valleys. The vantage point is the northwest corner of the spoil. The buried bedrock topography shown here has a pronounced

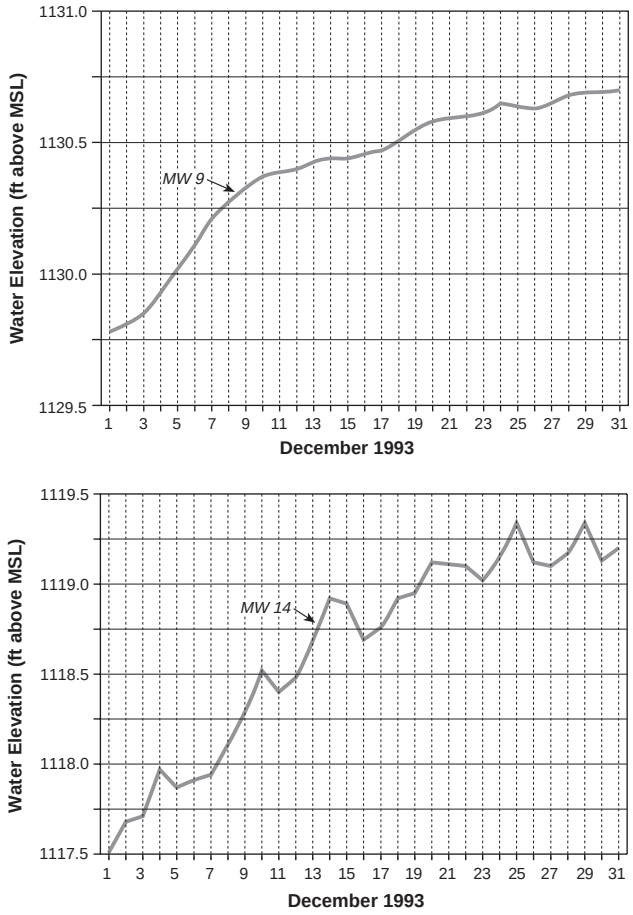

Figure 15. Hydrographs for monitoring wells 9 and 14 for December 1993.

effect on the occurrence and movement of ground water in the spoil.

Figure 19 shows several features and ground-water flow directions superimposed on an aerial photograph of the northwestern part of the mine site (top photograph). The vantage point is the same as in Figure 18. Water contained in the valley fills flows toward the northwest, where it discharges at springs. Water that accumulates in the southeastern part of the spoil's interior flows toward the heads of the buried valleys, which are now valley fills. This is evidenced by dye-trace data, head data, and the bottom structure of the buried plateau. Some of the water in the spoil's interior discharges to ponds situated above the springs on the northwest face. These points of discharge are illustrated in the bottom photograph of Figure 19, an aerial photograph with a close-up view of the northwest face of the spoil. Water entering the spoil through the infiltration basin (not within view in either photograph in Figure 19) probably flows into Spring Gap, as previously indicated by the dye-trace and head data from the wells surrounding the basin. The pond water, in turn, flows

Table 3. Hydraulic conductivity in monitoring wells, measured by slug tests.

Well No.	*Hydraulic Conductivity (cm/sec)*	*Hydraulic Conductivity (ft/sec)*
MW 4	7.0×10^{-5}	2.0×10^{-6}
MW 5	$> 8.2 \times 10^{-4}$	$> 2.7 \times 10^{-5}$
MW 7	2.0×10^{-5}	8.0×10^{-6}
MW 8	$> 7.3 \times 10^{-4}$	$> 2.4 \times 10^{-5}$
MW 9	4.0×10^{-5}	1.0×10^{-6}
MW 10	$> 9.0 \times 10^{-4}$	$> 2.9 \times 10^{-5}$
MW 12	4.0×10^{-4}	1.0×10^{-5}
MW 13	$> 5.8 \times 10^{-4}$	$> 1.9 \times 10^{-5}$
MW 14	2.0×10^{-4}	8.0×10^{-6}

down the face of the spoil, where it joins with the spring discharge before entering the lowermost sediment pond (Fig. 19, top photograph).

Mass-balance calculations indicate that the amount of water contributed by the pond overflow to the total mine outflow (0.86 cfs) is less than the amount of water that discharges from the valley fills (1.39 cfs). Water recharging the buried Spring Gap and Long Fork valleys is supplied from (1) ground water derived from bedrock along the valley fills at the spoil-bedrock contact, (2) surface-water seepage along the spoil-bedrock contact, and (3) the capture of ground water from the spoil's interior in the southeastern part of the spoil.

Figure 20 is a map of the spoil body; the arrows indicate the assumed direction of ground-water flow. It represents a conceptual model of ground-water movement through the spoil.

In this model the majority of water moves through the valley fills around the main spoil body and discharges at the northwest corner of the spoil. Recharge enters the spoil mainly along the edges of the valley fills, and at discrete points on the reclaimed surface, which includes the infiltration basin.

HYDROGEOCHEMISTRY

WATER-MINERAL REACTIONS

The mineralogy of the overburden plays an important part in determining chemical evolution of ground water in mine spoil. In addition, the mining process exposes unweathered mineral surfaces and increases the potential reactive surface area. Several dominant chemical reactions occur in almost all

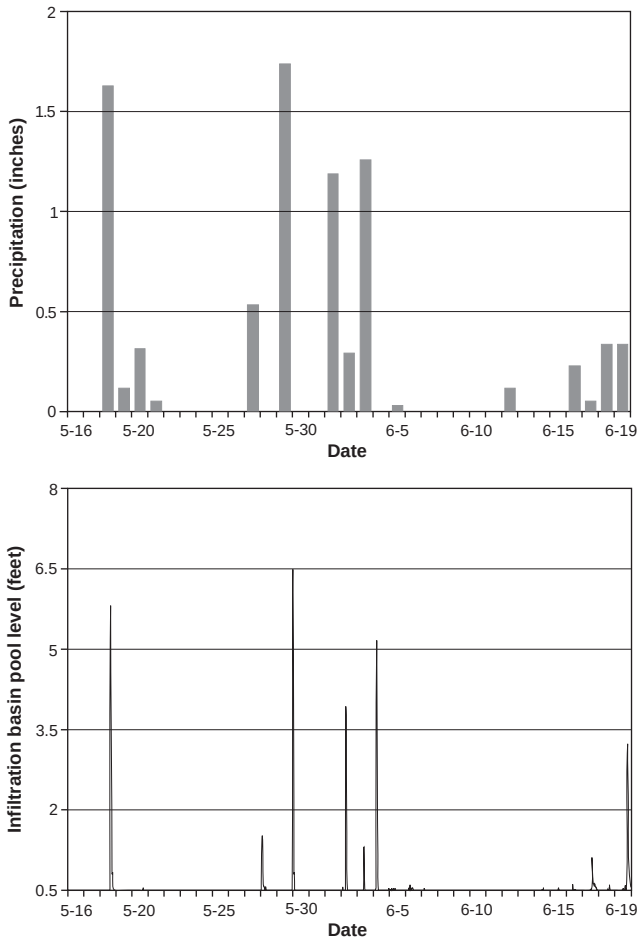

Figure 16. Response of pool elevation in infiltration basin to precipitation events from May 16 through June 19, 1991.

geologic terranes that contain coal, and these reactions have a great impact on the major dissolved constituents in ground and surface water (Williams and Hammond, 1988).

High concentrations of sulfate in ground and surface water are often associated with coal mining. The most probable source of sulfate in eastern Kentucky is from the oxidation of iron sulfide minerals. Both pyrite and marcasite are common iron sulfide minerals in the Appalachian coal field (Powell and Larson, 1985). Sulfate-bearing minerals such as gypsum ($CaSO_4 \cdot 2H_2O$) are not common primary minerals in the rocks of eastern Kentucky; therefore, the dissolution of gypsum probably is not a major source of sulfate.

Generally, the oxidation of pyrite can be represented as follows:

$$2FeS_2 + 7O_2 + 2H_2O \rightarrow 2Fe^{2+} + 2H_2SO_4 + 2SO_4^{2-}$$

Additional excess acidity can be generated if conditions within the spoil are conducive to the establishment of a population of iron-oxidizing bacteria such as *Thiobacillus ferrooxidans* (Singer and Stumm, 1970), which catalyze the reactions that produce acid-mine drainage. The resulting sulfuric acid solution can react with carbonate minerals (e.g., calcite), resulting in the neutralization of the acid and the release of calcium and sulfate, along with an increase in bicarbonate. The net reaction is as follows:

$$2CaCO_3 + H_2SO_4 \rightarrow 2HCO_3^- + 2Ca^{2+} + SO_4^{2-}$$

Dolomite is rare in the rocks of the Breathitt Formation (Danilchik and Waldrop, 1978; Weinheimer, 1983), and therefore the dissolution of this mineral probably does not contribute magnesium, which is found in significant concentrations in the spoil's ground water.

Chlorite ($(Mg,Fe)_6(AlSi_3)O_{10}(OH)_8$) is common in Breathitt rocks (Papp, 1976; Weinheimer, 1983), and it may be a significant source of magnesium in ground water (Hem, 1985). The weathering of chlorite is promoted by acidic conditions, making this reaction likely in areas where pyrite oxidation occurs (Powell and Larson, 1985).

Cation exchange is a geochemical process that may affect the distribution of cations in ground water in contact with mine spoil. In spoil water laden with divalent cations, the most likely reaction is one in which the preferred divalent cations such as calcium and magnesium are exchanged for sodium on the surfaces of reactive clays, iron hydroxides, or organic matter present in the spoil. The net effect is to increase the sodium concentration relative to the divalent cations in the ground water. The reaction is shown below, with X representing the exchange site on the solid:

$$2NaX + Ca^{2+} \rightarrow 2Na^{+} + CaX$$

An additional reaction is the chemical weathering of silicate minerals such as feldspars and clays, which tends to release alkali-metal cations, silica, and bicarbonate into solution (Freeze and Cherry, 1979; Powell and Larson, 1985).

Interpretation of Spoil-Water Data

Figure 21 is a trilinear diagram in which the results of analyses of water samples are plotted as a function of the normalized percentage of the samples' major cations and anions. Sixty-eight water samples are represented on the diagram, including all ground-water samples taken from monitoring wells and springs from April 1991 through June 1992. Chemical data for each sample are listed in Appendix A. All samples plot in the same general location on the diamond-shaped field of the diagram, indicating that they possess the same distribution of major ions. The dominant cations are calcium and magnesium, and sulfate is the dominant anion. The data shown represent four sampling events spanning 14 months, indicating that the water composition at the site var-

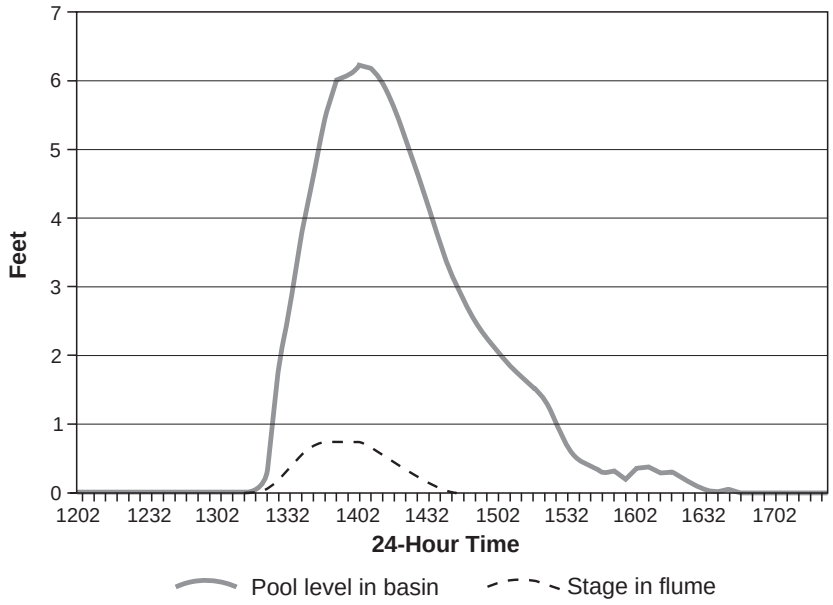

Figure 17. Relationship between flume stage and pool level during and after the May 29, 1991, storm.

ies little temporally. The most likely origin for the calcium-magnesium-sulfate water type at the site is the oxidation of iron sulfide minerals with the contemporaneous dissolution of calcium carbonate. The source of the relatively high amounts of magnesium is not well understood, but high-magnesium calcite or magnesium-rich clays such as illite or chlorite could be potential sources.

Figure 22 shows the distribution of pH values for all monitoring wells and spring 1. Most of the monitoring wells have maximum, median, and minimum pH values greater than 6.0, except for wells 6, 11, and 14. Overall, the majority of groundwater samples collected at the site indicate that the mine spoil generally does not produce highly acidic water.

Samples from MW 14 all have a pH of less than 4.5, which represents the lowest pH measurements encountered on the site. Samples taken from MW 14 are somewhat separated from the other samples plotted on the trilinear diagram (Fig. 21). The distribution of cations (mainly calcium and magnesium) is consistent with the distributions found in other well samples, the major difference being in the distribution of the anions. In MW 14 the dominant ion is sulfate, but the anionic distribution differs from that of the other wells by containing very low amounts of bicarbonate.

Water samples from MW 14 have bicarbonate contents lower than the other water samples by approximately two orders of magnitude. The range of bicarbonate concentration in MW 14 is from 3.66 to 8.54 mg/L, and the range of bicarbonate in samples from all other wells is from 185 to 1,046 mg/L.

A plausible explanation for the low bicarbonate level is that MW 14 collects water from an area where the rocks contain significant amounts of sulfide-bearing minerals and conditions are favorable for their oxidation. In addition, the amount of sulfide minerals in the vicinity of this well must be much greater than the amount of calcium carbonate. In this case, excess sulfuric acid would be produced, resulting in low bicarbonate concentrations and low pH.

Well 14 is located over a valley fill and is near a recharge area where Kemp (1990) observed surface water accumulating at the spoil-highwall contact. The highest average Eh value (mean Eh=398 millivolts [mV]; coefficient of variation=3.3 percent) of all the wells surveyed was observed at MW 14, and is in the Eh range in which the oxidation of sulfides is likely to take place (Champ and others, 1979). In addition, MW 14 is adjacent to an experimental goose pond situated on the reclaimed spoil. The pond has been prone to leaking, which could supply oxygen-rich surface water to the saturated zone monitored by MW 14. The result would be a geochemical environment that could create the acidic water encountered in MW 14. However, iron concentrations are lower than expected if pyrite is actively being oxidized and dissolved. One explanation for the relatively low iron concentration could be the contemporaneous precipitation of hydrous ferric hydroxides along the water's flow path.

Wells 4 and 7 had the highest average dissolved iron contents of 39.1 and 44.1 mg/L, respectively. MW 7 is directly downgradient from the point where Chestnut Gap Branch disappears into the spoil, and MW 4 is downgradient from the recharge water that enters the spoil through the infiltration basin. Chemical data show that these two wells also had the lowest average Eh measurements (213 and 159 mV, respectively). These values indicate slightly oxidizing to reducing conditions, which means conditions are more conducive for sustaining high dissolved iron concentrations in ground water in this area than in other areas of the spoil (Domenico and Schwartz, 1990). The relatively low Eh conditions may be related to the consumption of oxygen during the oxidation of

Table 4. Water levels in wells near the infiltration basin.

Date	*MW 2*	*MW 4*	*MW 5*
3/13/91	1132.5	1128.4	1131.9
6/20/91	1132.0	1128.4	1132.4
7/17/91	1132.7	1128.6	1133.3

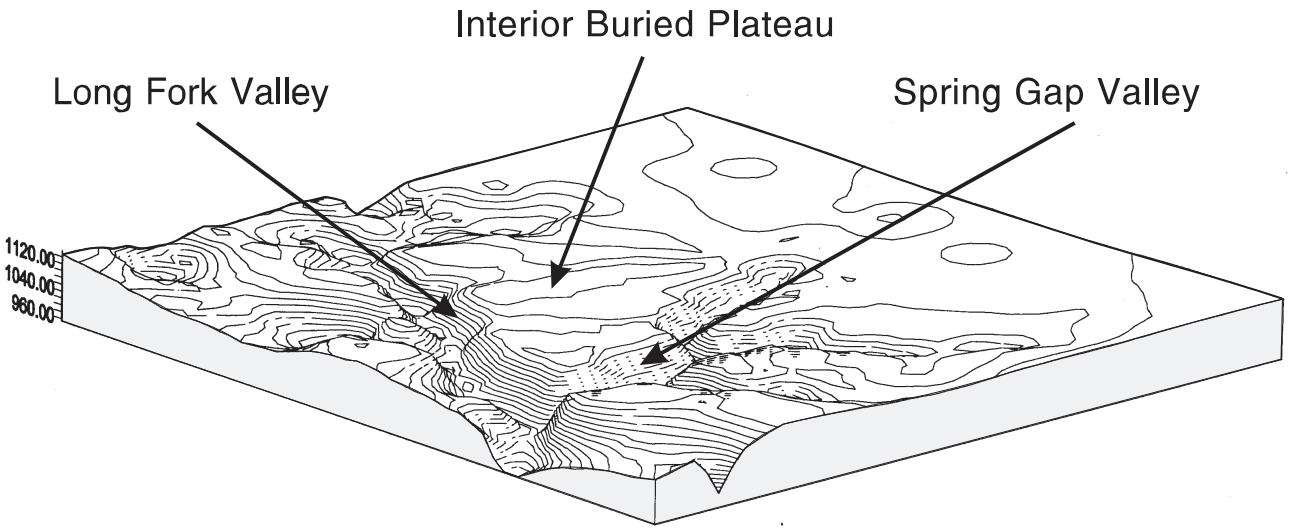

Figure 18. Digital terrain model showing the bedrock topography buried beneath the spoil. Features such as the buried plateau and the Spring Gap and Long Fork valley fills can be seen in Figure 19. Vantage point is from the northwestern corner.

organic matter. Both wells 4 and 7 are directly downgradient from points of surface-water recharge that are likely to contain water with more organic components than water from other locations that flows over the relatively sterile, unvegetated spoil. Surface water entering the spoil near MW 7 (i.e., Chestnut Gap Branch) flows through an unmined valley used for cattle grazing, where organic matter from decaying vegetation or from animal waste is likely to occur. The drainage basin surrounding the infiltration basin is well vegetated at the time of the writing of this report compared to most of the reclaimed spoil. Organic matter acts as a food source for bacteria, aids in the consumption of dissolved oxygen in the ground-water system, and can form organic-metallic complexes. These and other processes can affect the solubility and mobility of dissolved iron (Domenico and Schwartz, 1990). More chemical data are needed to confirm or discount these hypotheses concerning water chemistry at the site.

Head distribution for wells on the periphery of the infiltration basin indicates that water entering the spoil through the basin moves toward MW 4. This is substantiated by chemical data from water samples taken from wells 2, 4, and 5. The average TDS content of the samples taken from MW 4 is 789 mg/L (see Appendix A for chemical data), which is approximately one-third the TDS values of the other wells surrounding the infiltration basin (MW 2 and MW 5). TDS values for wells 2 and 5 are similar to each other (average TDS values are 2,273 and 2,216 mg/L, respectively). The lower TDS value in MW 4 is most likely a result of dilution by the less mineralized surface water entering the spoil through the infiltration basin. A sample of water taken from the intermittent flow that descends into the infiltration basin had a relatively low dissolved solid content (177.8 mg/L) and a pH of 7.67. We can reasonably assume that the majority of surface water entering the basin is similar in chemistry to this sample. Unless disturbed, the spoil exposed at the surface will become less and less reactive because of leaching by subsequent precipitation. Therefore, the low TDS values of water samples from MW 4 probably reflect the mixing of recharge water entering through the infiltration basin and more mineralized ground water in the saturated zone.

The mean TDS value (see Appendix A) for wells in the interior plateau region of the spoil (2, 3, 5, 8, 9, 11, 12, and 13) is 2,474 mg/L (standard deviation=349), whereas mean TDS values for the valley-fill wells (4, 6, 7, 10, 14) and spring 1 is 1,414 mg/L (standard deviation=820). The higher TDS values characteristic of the interior of the spoil are most likely the result of longer contact time between slowly moving ground water and reactive spoil. The extended contact time allows for greater water-rock interaction and leaching of soluble and reactive rock materials, which results in an increase in the total concentration of the dissolved constituents.

Limited data indicate that the TDS concentration of the water entering the spoil at Chestnut Gap Branch is generally lower than that of the water emerging from the springs (data from SP 1 in Appendix A) at the discharge zone. Discharging ground water from SP 1 has a TDS content nearly three times that of the water entering the spoil at Chestnut Gap Branch. This dramatic increase in mineralization probably results from two main processes: (1) the recharging water, although only in contact with the spoil material for a short time (as evidenced by travel times determined by dye-tracing), reacts with minerals in the spoil, and (2) the relatively fresh water from the stream is mixing with the more mineralized water entering the valley fills from the interior of the spoil. Mass-balance calculations demonstrate that the mixing

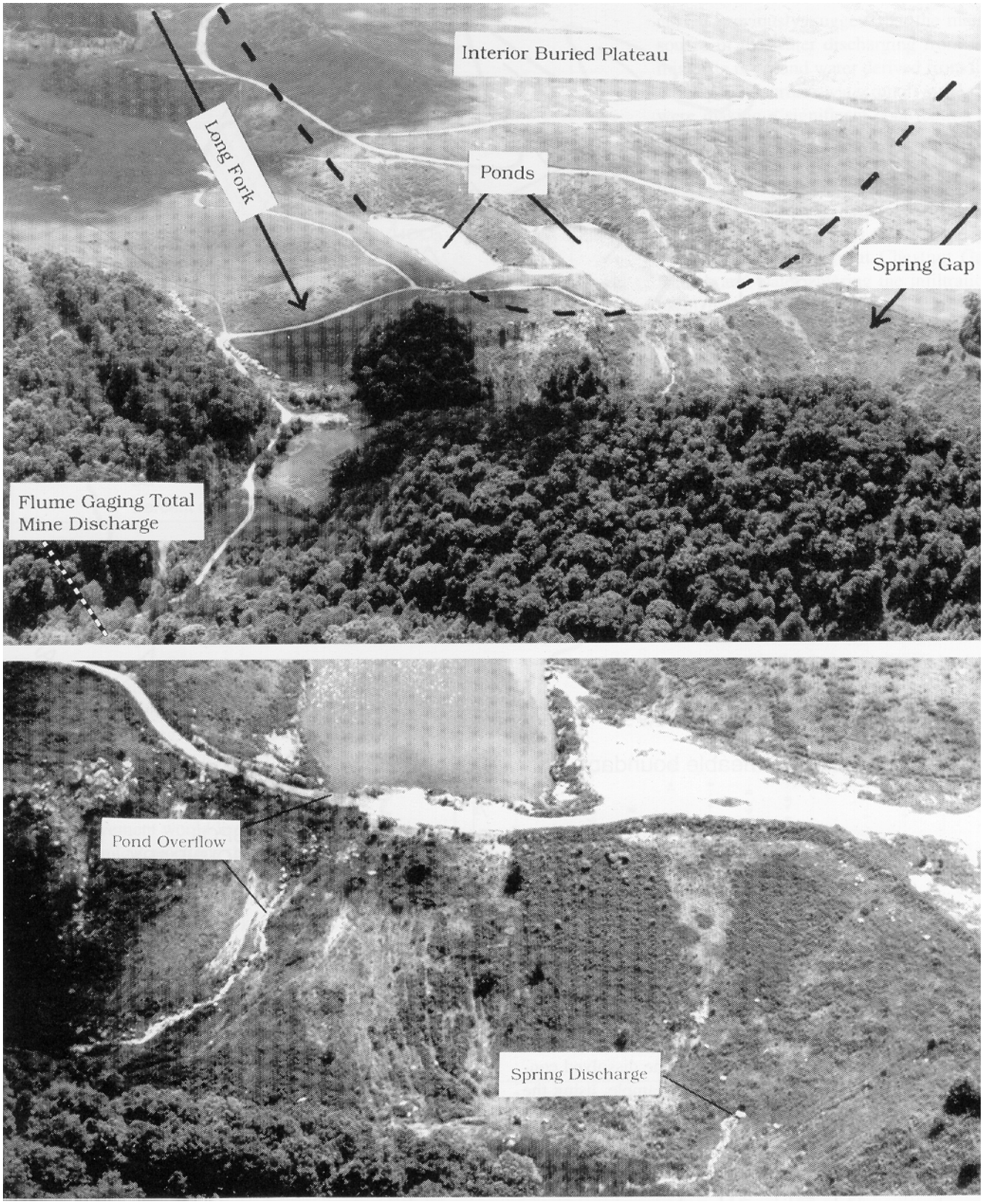

Figure 19. Aerial photographs of the northwest corner of the reclaimed mine site. The conceptual ground-water flow system is superimposed on the top photograph. Ground-water discharge points along the northwest slope of the spoil body are superimposed on the bottom photograph.

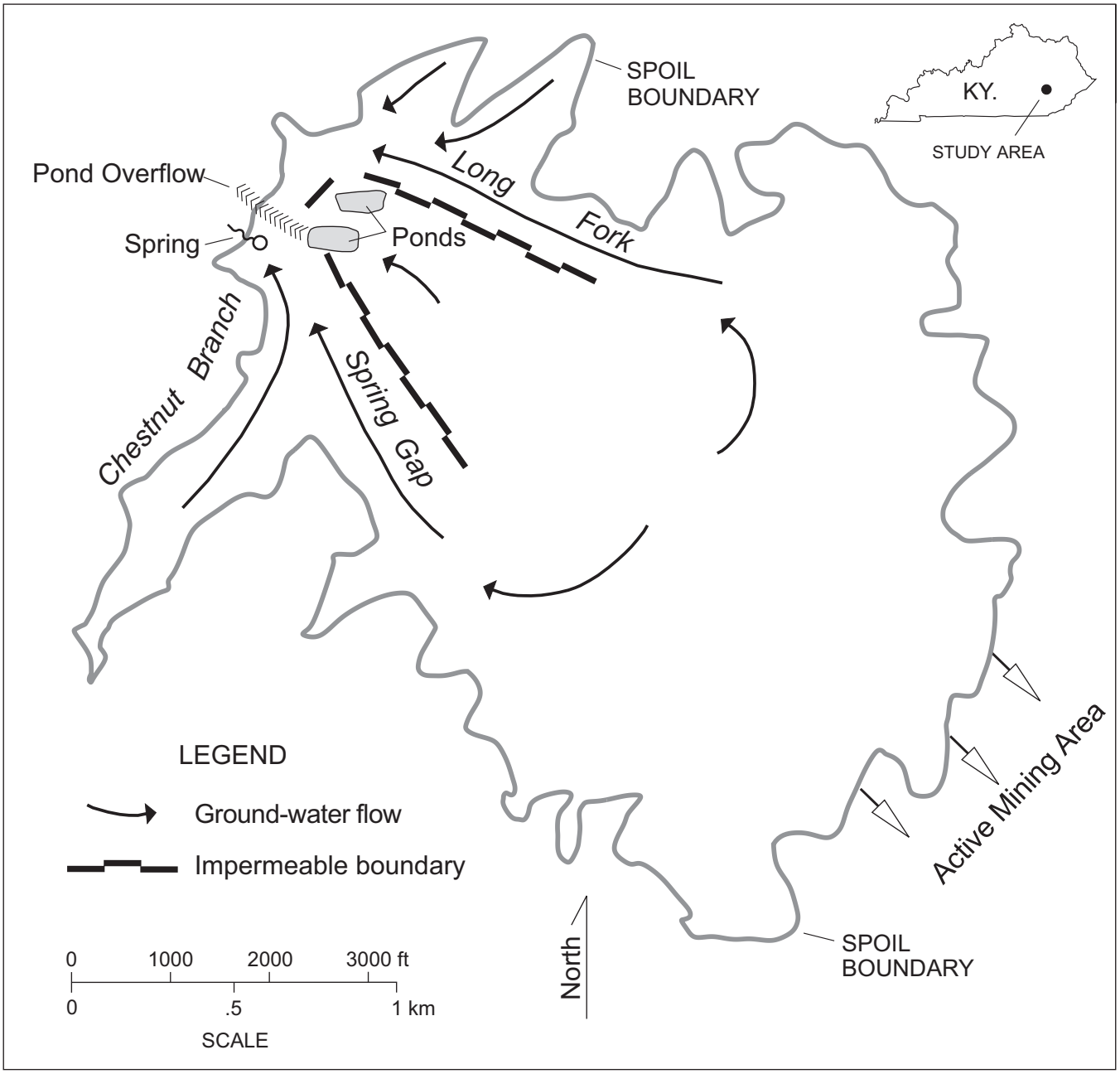

Figure 20. Conceptual model of ground-water flow in the spoil at the Star Fire site. Direction of flow is uncertain near the active mining area.

scenario can account for the majority of the dissolved constituent load measured at spring 1. For example, using the TDS data from June 1994 and the surface-water flow data used in previous calculations, the expression for the mass loading at spring 1 is:

$$Q_{sp} C_{sp} = Q_{cb} C_{cb} + Q_{(sp-cb)} C_{spl}$$

where C_{spl} is the TDS load of water in the Spring Gap valley fill, which would mix with water entering the spoil from Chestnut Gap Branch. Solving for C_{spl} yields a TDS concentration of 2,378 mg/L. Monitoring well 7 is located approximately 700 feet upgradient from spring 1, and is probably a good indicator of the TDS concentration of water originating from the interior spoil and presently stored in the Spring Gap valley fill. The measured TDS value from MW 7 is 2,740 mg/L, and is within 13 percent of the calculated value. This example suggests that ground-water mixing is occurring, and that mix-

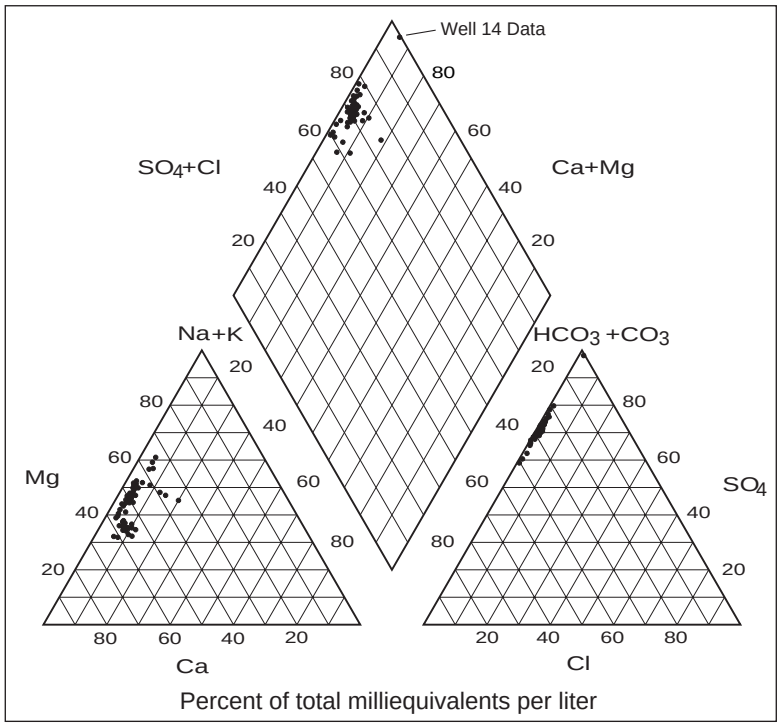

Figure 21. Piper diagram showing the water types of samples from monitoring wells 2 through 14 and the main spring.

ing is an important determining factor for water quality in the spring. This is a reasonable interpretation, considering that Kemp (1990) demonstrated that travel time for water entering the spoil at Chestnut Gap Branch and discharging at spring 1 is less than 73 hours. This rapid rate of water movement would limit the amount of time for chemical reactions that increase TDS concentrations, especially if channelized flow controls the movement of ground water in the spoil. Channelized, or pseudo-karstic, flow can limit the amount of spoil-water contact that adds dissolved solids to water moving through the spoil (Caruccio and Geidel, 1984).

TDS data indicate that the majority of the water leaving the site is derived from the spoil. Based on average TDS values, wells 7 and 10, which are closest to the flume monitoring the mine outflow in Long Fork (see Fig. 7 for the location), yield TDS concentrations very similar to the TDS concentration of water discharging the mine site through the Long Fork flume (TDS values are 2,573 and 1,966 mg/L for wells 7 and 10, respectively, and 1,947 mg/L for the flume). These data, along with the mass-balance calculations for the total water budget discussed previously, suggest that the major source of the water discharging from the mine site is ground water derived from the mine spoil. If surface-water runoff at the site were making a significant contribution to the total mine outflow, the TDS measured at the outflow would be considerably less than that observed for spoil ground water, because of dilution. Samples of surface water collected at other areas of the site (e.g., water from the stream at Chestnut Gap Branch and water entering the infiltration basin) have TDS concentrations that are generally less than 600 mg/L (Dinger and others, 1990).

Table 5 gives the saturation indices (IAP/K) calculated for several minerals that may affect the water chemistry of the spoil ground water. Degree of saturation is defined in terms of the saturation index (SI):

$$SI = \text{Log}\frac{IAP}{K}$$

where IAP is the ion activity product and K is the equilibrium constant of the mineral in question. If the SI is less than zero, the so-

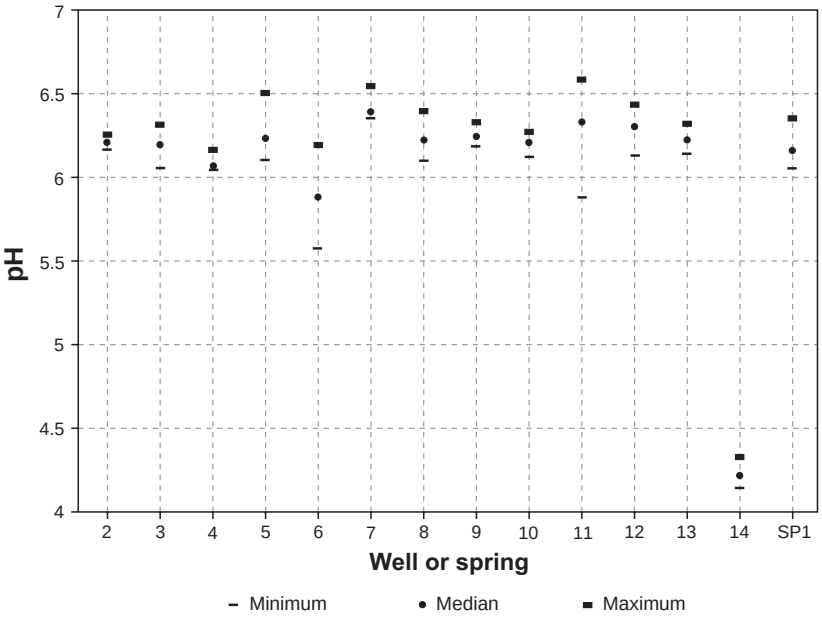

Figure 22. Distribution of pH values for water samples collected from monitoring wells and SP 1.

Table 5. Saturation indices (log IAP/K) determined by PHREEQE for minerals of interest.

Location	Calcite	Gypsum	Siderite	Kaolinite	Illite	Chlorite	Pyrite	Microcline
MW 2	-0.3618	0.0116	-0.6845	6.2203	1.6237	-10.9561	-22.1385	1.6708
MW 3	-0.2230	0.0364	-1.1843	6.4020	1.9898	-10.8265	-43.2755	1.9905
MW 4	-1.2823	-0.8279	0.2801	5.5224	-0.0222	-15.3130	-19.4716	0.211
MW 5	-0.2750	-0.0378	-1.5262	6.4527	1.9545	-10.2089	-48.4424	1.7998
MW 6	-1.5691	-0.8140	-0.8733	5.2917	-0.5484	-17.2109	-31.5412	-0.2483
MW 7	-0.2747	0.0095	0.9464	6.7562	2.6430	-7.3621	-4.5329	2.3076
MW 8	-0.0049	0.0754	0.0248	6.7434	2.6834	-7.8246	-27.4105	2.3751
MW 9	-0.2792	-0.0681	-0.9093	6.4664	2.0648	-9.2461	-25.0982	1.8463
MW 10	-0.4647	-0.1012	-1.0106	6.2025	1.5560	-10.3842	-32.2609	1.4937
MW 11	-0.5093	0.1195	-0.2456	6.2857	1.6712	-12.3585	-16.7571	1.6814
MW 12	-0.2738	0.1251	-0.7852	6.3829	1.8905	-11.3047	-34.8944	1.8854
MW 13	-0.4078	-0.0217	-0.1397	6.8662	2.3590	-9.9278	-30.1142	1.8613
MW 14	-4.5345	-0.4288	-4.0317	3.5229	-4.1189	-34.2911	-39.3488	-2.4135
SPRING	-2.4520	-0.0336	-4.1911	6.0570	1.3376	-11.5458	-48.6748	1.4553

lution is undersaturated with respect to a given mineral and the mineral may dissolve. If the SI is equal to zero, the solution is at equilibrium. If the SI is greater than zero, the solution is supersaturated, and the mineral should precipitate from the solution.

Saturation indices for minerals of interest were calculated using the geochemical model PHREEQE (Parkhurst and others, 1980). Data used in the calculations were from water samples collected on June 16, 1992. These data were chosen because of the high quality of the analyses: the ion charge-balance error was less than 6.2 percent for all samples, and the mean error for the 14 samples was 2.3 percent.

These data indicate that all water samples are undersaturated with respect to pyrite, which is assumed to be the major source of iron, sulfate, and acidity. The samples are also undersaturated with respect to calcite: if present, calcite should dissolve. Often, calcite cements in sandstones are magnesian calcite, and the dissolution of these cements could provide both calcium and magnesium to the ground water (Hem, 1985). Siderite ($FeCO_3$), which is found as concretions in shales (Danilchik and Waldrop, 1978) and as a cement in sandstones (Weinheimer, 1983), is undersaturated in all wells except wells 4, 7, and 8. The dissolution of siderite would also add bicarbonate alkalinity to the ground-water system when it reacted with acidic water from pyrite oxidation. Powell and Larson (1985) found chlorite to be a probable source of magnesium in ground water derived from rocks that are stratigraphically and lithologically similar to the rocks that compose the overburden at the Star Fire site. The phyllosilicate mineral chlorite is present in the overburden (Papp, 1976), and is probably the major source of magnesium. The saturation indices for chlorite indicate that this mineral is also undersaturated in the spoil ground water. Thus, the equilibrium data are consistent with this assessment.

The state of water saturation with respect to gypsum must be considered because of the high concentrations of both calcium and sulfate in the spoil ground water. Figure 23 shows the saturation indices for gypsum for each well and spring 1. Wells 4, 5, 6, 9, 10, 13, and 14 are all undersaturated with respect to gypsum. Wells 4, 6, and 14 are vastly undersaturated. As discussed previously, each of these three monitoring wells is located in areas where direct recharge from surface water is evident. Dilution by surface water is the most likely explanation for the high degree of gypsum undersaturation in these wells. TDS data shown in Appendix A provide evidence for this explanation. Total dissolved solid averages for these three wells are the three lowest values from all wells at the site; this is probably the result of dilution with less mineralized surface water. Moreover, the percentage distribution of cations and anions for samples from these three

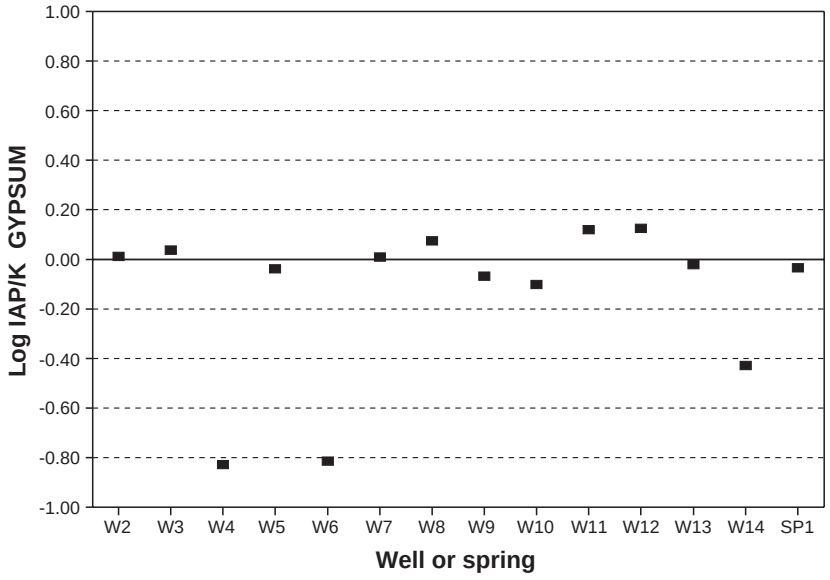

Figure 23. Saturation indices (IAP/K) for gypsum ($CaSO_4 \cdot 2H_20$) for water samples collected in June 1992.

wells is consistent with that of all other ground-water samples, which also indicates dilution.

Samples from wells 2, 3, 7, 8, 11, and 12 are saturated with respect to gypsum. Each of these wells, except for MW 7, is located in the interior of the spoil. Wells 8 and 11 have some of the highest TDS concentrations observed at the site (see Appendix A). The degree of gypsum saturation in these wells correlates well with the increased mineralization of the ground water in the spoil's interior.

Sodium and potassium concentrations are generally low compared to the calcium and magnesium concentrations in all samples. Cation exchange, therefore, is probably not an important factor in determining the water type at the site. Other sources for sodium and potassium may result from the weathering of silicate minerals. However, the saturation indices for kaolinite, illite, and microcline indicate saturation in most of the samples representative of the spoil ground water. Only in very acidic conditions should chemical weathering of these silicates become significant. For example, very acidic conditions were consistently found in MW 14, and both illite and microcline are undersaturated, and would be expected to dissolve. However, the kinetics of dissolution of these minerals is slow (Powell and Larson, 1985), and therefore their dissolution is probably unimportant to the overall chemistry of ground water at the site.

Spoil Settlement

Table 6 contains the spoil-settlement data collected in 1992 and 1993. Figure 24 shows settlement that occurred subsequent to well installation, measured in tenths of a foot, based on the two data sets. A good correlation exists between the age and thickness of spoil and areas of high settlement. The northwestern area of the spoil has been in place the longest time: parts of the valley fills in Spring Gap and Long Fork have been in place for over 10 years. This area showed the least settlement, generally 0.2 to 0.4 ft during the period of observation. The area of maximum settlement occurred in the southeastern part of the spoil, where active mining is producing recent spoil. The maximum settlement that occurred between the time of well installation (July and August 1990) and November 1993 was 0.92 ft near MW 11, which translates into an average settlement rate of approximately 0.28 ft per year.

The contour lines in Figure 24 also indicate a lobe of higher settlement in the spoil overlying the buried plateau. This is the area where the spoil is the thickest, and in some places it exceeds 250 ft (Kemp, 1990). However, the limited data here do not allow determination of which variable is the most important factor in predicting where maximum settlement will occur (age, thickness, or subsurface geometry).

The settlement rate calculated here is based merely on an arithmetic average of settlement per unit time. In addition, spoil measurements did not commence with the initial placement of the spoil immediately after mining. Settlement rates for earthen materials such as mine spoil usually decrease at an exponential rate (Charles and others, 1977). Therefore, the amount and rate of settlement at the Star Fire site should decrease substantially with time. Additional study is needed.

Summary

Mine spoil at the Star Fire site ranges from approximately 100 to 300 ft in thickness. Selected spoil handling techniques, such as cast blasting, dragline casting, and dumping by trucks, is providing a framework for water storage in the 1,000 acres that have been mined at the Star Fire site.

Field investigations have identified numerous ground-water recharge and discharge zones at the mine spoil area. Recharge occurs by way of disappearing streams, ground-water infiltration along exposed boulder zones, and at areas where the spoil is in contact with the bedrock highwalls. Minor recharge occurs locally on the spoil's surface through macropores (snakeholes). Discharge of ground water from the spoil occurs mainly through springs and seeps at the outslope of the spoil body. Ground-water movement within the spoil is controlled by the ground-water gradients within the spoil, which are a function of the buried topography and the interaction of the recharge and discharge zones with zones of low-permeability spoil. The spoil interior, lacking any major

Table 6. Measurements of settlement around monitoring wells (tenths of feet). Wells installed July–August 1990.

July 1992					
Well ID	*North*	*East*	*South*	*West*	*Mean*
MW 4	0.67	0.63	0.56	0.52	0.59
MW 5	0.46	0.75	0.73	0.58	0.63
MW 6	0.27	0.23	0.17	0.17	0.21
MW 7	0.20	0.25	0.15	0.11	0.18
MW 8	0.60	0.52	0.42	0.55	0.52
MW 9	0.36	0.33	0.31	0.43	0.36
MW 10	0.00	0.04	0.00	0.04	0.02
MW 11	0.67	0.79	0.65	0.59	0.67
MW 12	0.38	0.42	0.40	0.21	0.35
MW 13	0.40	0.49	0.53	0.44	0.46
MW 14	0.21	0.30	0.31	0.28	0.28
November 1993					
Well ID	*North*	*East*	*South*	*West*	*Mean*
MW 4	0.82	0.80	0.65	0.64	0.73
MW 5	0.57	0.80	0.90	0.74	0.75
MW 6	0.30	0.28	0.20	0.10	0.22
MW 7	0.28	0.34	0.24	0.22	0.27
MW 8	0.70	0.72	0.52	0.60	0.64
MW 9	0.25	0.23	0.11	0.23	0.21
MW 10	0.14	0.03	0.05	0.06	0.07
MW 11	0.95	0.90	0.93	0.90	0.92
MW 12	0.70	0.85	0.92	0.87	0.84
MW 13	0.53	0.52	0.70	0.65	0.60
MW 14	0.23	0.40	0.30	0.30	0.31

direct recharge from the surface, slowly accumulates water, whereas in the valley fills ground water moves at a rapid rate. Recharge to the valley fills comes from streams, adjacent bedrock aquifers, and from surface water that seeps in near the bedrock-spoil interface.

Water-table elevations measured at monitoring wells, springs, and ponds indicate that a saturated zone in the interior of the spoil slowly discharges to the southeast or northwest, and that two additional saturated zones occur at lower elevations in the two adjoining valley fills (Spring Gap-Chestnut Gap Branch and Long Fork). Most likely, these saturated zones are in hydraulic connection in the upper reaches (southeastern part) of the spoil body, but are separated by the topography of the basal bedrock in the central plateau section of the spoil.

Based on an average saturated thickness of 21 ft and a spoil porosity of 20 percent for the site, an estimated 4,200 acre-ft (1.4 billion gallons) of water exists in the 1,000-acre spoil. The average saturated thickness of the wells located in the valley fills (30.1 ft) is nearly twice that (15.4 ft) for the wells located in the spoil's interior.

The range of hydraulic conductivity values computed in the spoil are from 2.0×10^{-6} to more than 2.9×10^{-5} ft/sec. The upper limit of K for spoil wells could not be determined because of equipment limitations; thus, the upper range could be significantly higher than measured. Because there is no discernible difference in hydraulic conductivity between the wells in the valley fills and wells in the spoil interior, the apparently sluggish ground-water movement in the spoil interior must be related to gradients induced by recharge-discharge relationships.

A deep infiltration basin instrumented at the site collects surface runoff from the spoil. A 1.64-inch precipitation event produced 24,390 ft^3 (182,000 gallons) of runoff, which entered the spoil through the infiltration basin at an average rate of 136 ft^3 (1,010 gallons) per minute. The head distribution measured in monitoring wells around the infiltration basin indicates that the water entering the basin is flowing toward the Spring Gap valley fill and most likely discharges from the springs in the northwestern part of the spoil.

Chemical analysis of samples from monitoring wells and springs shows that all waters at the site are a calcium-magnesium-sulfate type. The pH of all ground-water samples, except for those from MW 14, fell into a favorable range of approximately 6 to 7. The TDS values for wells located in the spoil interior are higher than the average value for wells located in the valley fills. Higher mineralization of the water samples from the interior spoil area probably reflects the longer contact time of ground water with reactive spoil material, as inferred from the gentle gradient of the water table and dye-tracing data. Lower TDS values for the valley-fill wells probably result from a greater contribution of less mineralized surface water into the ground-water flow system and a shorter residence time.

Ground-water chemistry appears to be controlled by the dissolution of calcite and probably weathering of chlorite, and the oxidation of sulfide minerals, resulting in a calcium-magnesium-sulfate water type for both ground and surface water at the site. Most of the ground water in the spoil is at or

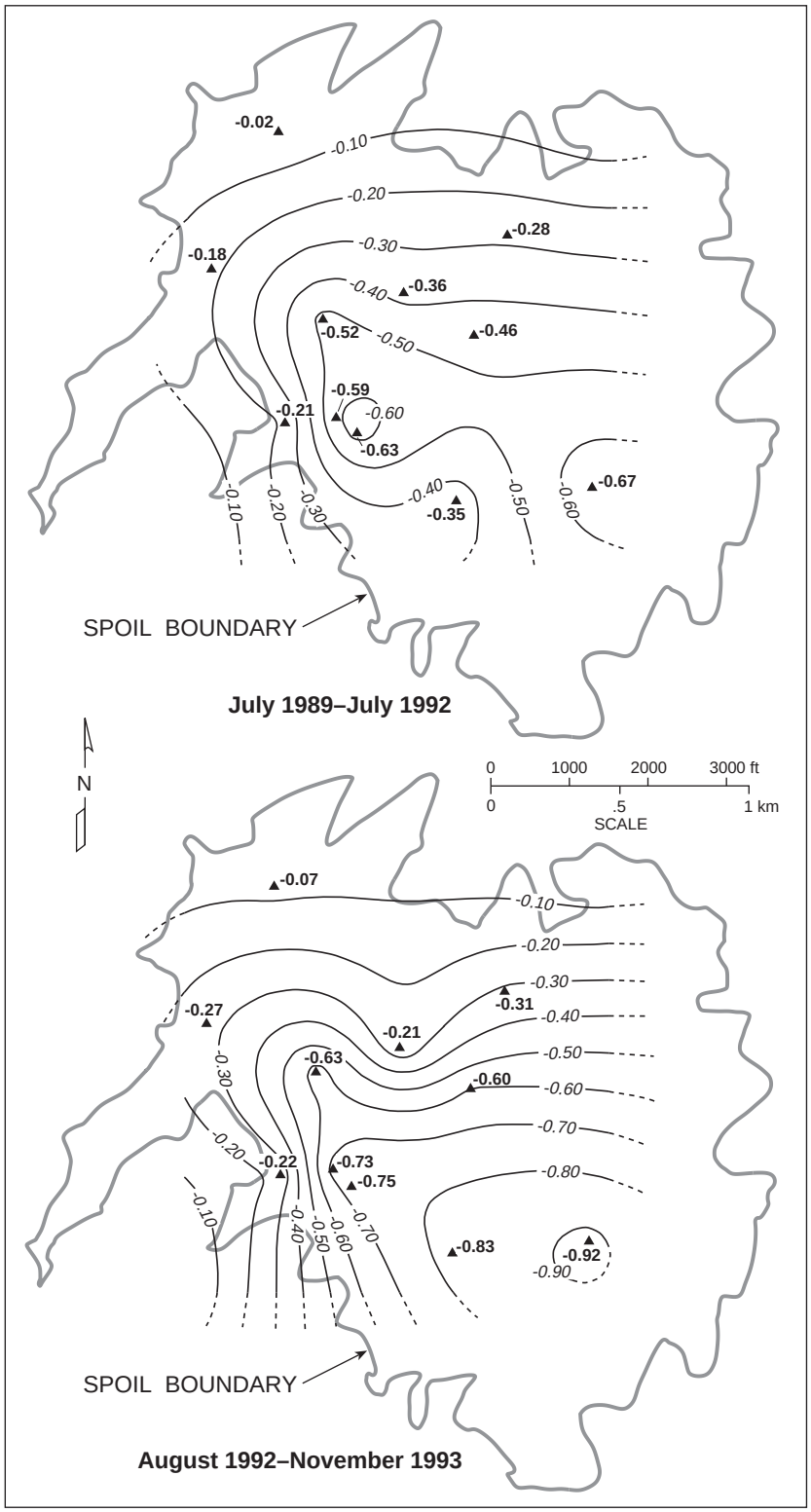

Figure 24. Mine spoil settlement around monitoring wells from July 1989–July 1992 and from August 1992–November 1993.

near equilibrium with the mineral gypsum. Some areas of the spoil, especially in valley fill areas near a bedrock highwall, are diluted by less mineralized surface water that can more easily infiltrate the spoil in these zones.

A conceptual model of ground-water flow patterns indicates that two separate but connected saturated zones occur in the spoil. Ground-water movement within the spoil is controlled by the gradients that form as a function of the interaction of recharge and discharge zones, by the topography of the relatively impermeable pavement that underlies the lowest coal being mined (Hazard No. 7), and by the drainage patterns that existed before mining began. The major streams that drained the premined area (Chestnut Gap Branch, Spring Gap, and Long Fork) eroded valleys whose bottoms are at elevations well below the level of the No. 7 coal. These drainage valleys became valley fills as contour-cut mining occurred along the valley walls. The interior of the spoil contains a relatively thin saturated zone from the accumulation of water from discrete infiltration zones within the spoil, the infiltration basin, and the active mining area where uncompacted or reclaimed spoil are present. Water that accumulates in the interior zone most likely flows into the valley fills on either side of the interior plateau in the upper reaches of the buried valleys in the southeastern section of the spoil, or flows to the northwest and discharges into either of the two ponds excavated into the bedrock pavement below the Hazard No. 7 coal.

Water in the valley fills receives contributions of ground water from the adjacent unmined bedrock highwall and surface water that accumulates and later percolates along the spoil-bedrock contact. The total mine outflow measured in the northwestern area of the reclaimed spoil produces a base flow of approximately 4 cfs (2.6 mgd). Variations in water quality observed at the site are related to the flow system described by this model.

Measurements taken at the spoil surface indicate that the spoil is exhibiting differential settlement related to the age and thickness of the spoil. The most recently mined areas of the spoil body exhibit the greatest settlement; the maximum spoil settlement rate observed was 0.28 ft per year.

Contour lines on maps of the spoil's water table and the spoil settlement are similar in that they both show changes in gradients that correlate with abrupt changes in topography defined by buried valleys and the pave-

ment bedrock resulting from coal extraction. This implies that the buried topography beneath large spoil areas such as the Star Fire site is important in predicting hydrologic and geotechnical characteristics of the spoil body, and must be considered when evaluating such sites.

The initial water-quality and -quantity data measured at the Star Fire Mine demonstrate that the ongoing mining techniques can provide the physical framework for water storage in the extensive mine spoil. Although the water stored in the spoil is not potable at this time, it likely could serve for various agricultural and industrial uses and may become more useful with time and as water-treatment technology improves. Development of a useful water supply within the spoil will be a key factor in future land use and economic diversity of the site and other similar sites in eastern Kentucky.

References Cited

Aldous, P.J., and Smart, P.L., 1987, Tracing ground water movement in abandoned coal mined aquifers using fluorescent dyes: Ground Water, v. 26, no. 2, p.172–178.

Aulenbach, D.B., Bull, J.H., and Middlesworth, B.C., 1978, Use of tracers to confirm ground-water flow: Ground Water, v. 16, no. 3, p. 149–157.

Caruccio, F.T., and Geidel, Gwendolyn, 1984, Induced alkaline recharge zones to mitigate acidic seeps, *in* Proceedings, 1984 Symposium on Surface Mining, Hydrology, Sedimentology, and Reclamation: Lexington, University of Kentucky, College of Engineering, College of Continuing Education and Extension, College of Agriculture–Department of Forestry, p. 43–47.

Champ, D.R., Gulens, J., and Jackson, R.E., 1979, Oxidation-reduction sequences in ground-water flow systems: Canadian Journal of Earth Science, v. 16, p. 12–23.

Charles, J.A., Naismith, W.A., and Burford, D., 1977, Settlement of backfill at Horslev restored opencast coal mining site, *in* Geddes, J.D., ed., Large ground movements and structures: New York, Wiley, p. 229–251.

Danilchik, Walter, and Waldrop, H.A., 1978, Geologic map of the Vest Quadrangle, eastern Kentucky: U.S. Geological Survey Geologic Quadrangle Map GQ-1141.

Diodato, D.M., and Parizek, R.R., 1994, Unsaturated hydraulic properties of reclaimed coal strip mines: Ground Water, v. 32, no. 1, p. 108–119.

Dinger, J.S., Warner, R.C., and Kemp, J.E., 1988, Building an aquifer in coal-mine spoil: Concept and initial construction at the Star Fire tract, eastern Kentucky, *in* Proceedings, 1988 Symposium on Surface Mining, Hydrology, Sedimentology, and Reclamation: Lexington, University of Kentucky, College of Engineering, College of Continuing Education and Extension, College of Agriculture–Department of Forestry, p. 85–93.

Dinger, J.S, Wunsch, D.R., and Kemp, J.E., 1990, Occurrence of ground water in mine spoil, a renewable resource: Star Fire tract, eastern Kentucky: Mining and Reclamation Conference and Exhibition, Charleston, W.Va., April 23–26, 1990, p. 171–179.

Domenico, P.A., and Schwartz, F.W., 1990, Physical and chemical hydrogeology: New York, Wiley, 824 p.

Freeze, R.A., and Cherry, J.A., 1979, Ground water: Englewood Cliffs, N.J., Prentice-Hall, 604 p.

Hem, J.D., 1985, Study and interpretation of chemical characteristics of natural water (3d ed.): U.S. Geological Survey Water-Supply Paper 2254, 263 p.

Herring, W.A., and Shanks, T.J., 1980, Hydraulic conductivity of cast overburden: EOS, v. 61, no. 48, p. 1193.

Hinrichs, E.N., 1978, Geologic map of the Noble Quadrangle, eastern Kentucky: U.S. Geological Survey Geologic Quadrangle Map GQ-1476.

Hvorslev, M.J., 1951, Time lag and soil permeability in ground-water observations: U.S. Army Corps of Engineers Waterways Experiment Station Bulletin 36.

Kemp, J.E., 1990, Hydrogeologic characterization of surface mine spoil, Star Fire Mine, eastern Kentucky: Lexington, University of Kentucky, M.S. Thesis, 102 p.

Kipp, J.A., and Dinger, J.S., 1991, Stress-relief fracture control of ground-water movement in the Appalachian Plateau: Kentucky Geological Survey, ser. 11, Reprint 30, 11 p.

Langmuir, Donald, 1971, Eh-pH determinations, *in* Carver, R.E., ed., Procedures in sedimentary petrology: New York, Wiley-Interscience, p. 597–634.

Oertel, A.O., and Hood, W.C., 1983, Changes in ground-water quality associated with cast overburden material in southwest Perry County, Illinois, *in* Proceedings, 1983 Symposium on Surface Mining, Hydrology, and Reclamation: Lexington, University of Kentucky, College of Engineering, College of Continuing Education and Extension, College of Agriculture–Department of Forestry, p. 73–78.

Papp, A.R., 1976, Extractable cations from claystones and shales of the Pennsylvanian Breathitt Formation in eastern Kentucky as related to depositional environments: Richmond, Eastern Kentucky University, M.S. Thesis, 153 p.

Parkhurst, D.L, Thorstenson, D.C., and Plummer, L.N., 1980, PHREEQE, a computer program for geochemical calculations: U.S. Geological Survey Water-Resources Investigation Report 80-96, 210 p.

Powell, J.D., and Larson, J.D., 1985, Relation between groundwater quality and mineralogy in the coal-producing Norton Formation of Buchanan County, Virginia: U.S. Geological Survey Water-Supply Paper 2274, 30 p.

Singer, P.C., and Stumm, Werner, 1970, Acidic mine drainage: The rate limiting step: Science, v. 167, p. 1121–1123.

Smart, P.L., and Laidlaw, I.M.S., 1977, An evaluation of some fluorescent dyes for water tracing: Water Resources Research, v. 13, p. 15–33.

Sobek, A.A., Schuller, A.J., Freeman, J.R., and Smith, R.M., 1978, Field and laboratory methods applicable to overburdens and minesoils: U.S. Environmental Protection Agency, EPA-600/2-78-054, 204 p.

Soil and Material Engineers, Inc., 1982, Ground water determination: Star Fire Coals, Inc., various pagination.

Spengler, R.W., 1977, Geologic map of the Salyersville South Quadrangle, Magoffin and Breathitt Counties, Kentucky: U.S. Geological Survey Geologic Quadrangle Map GQ-1373.

Taylor, P.B., 1995, Hydrologic assessment, SEDCAD+ model validation, and infiltration basin performance for the Appalachian coal region in Kentucky: Lexington, University of Kentucky, M.S. Thesis, 301 p.

Thompson, D.B., 1987, A microcomputer program for interpreting time-lag permeability tests: Ground Water, v. 25, no. 2. p. 212–218.

U.S. Geological Survey, 1980, National handbook for recommended methods for water-data acquisition; chapter 2—Ground water: U.S. Geological Survey Work Group 2, 147 p.

Weinheimer, R.L., 1983, Vertical sequence and diagenesis in Breathitt sandstones in eastern Kentucky: Cincinnati, Ohio, University of Cincinnati, M.S. Thesis, 147 p.

Williams, R.S., and Hammond, S.E., 1988, Soil-water hydrology and geochemistry of a coal spoil at a reclaimed surface mine in Routt County, Colorado: U.S. Geological Survey Water-Resources Investigations Report 86-4350, 100 p.

Wunsch, D.R., 1992, Ground-water geochemistry and its relationship to the flow system at an unmined site in the Eastern Kentucky Coal Field: Lexington, University of Kentucky, Ph.D. Dissertation, 239 p.

Wunsch, D.R., Dinger, J.S., and Taylor, P.B., 1992, Design, construction, and monitoring of the ground-water resources of a large spoil area: Star Fire tract, eastern Kentucky: Kentucky Geological Survey, ser. 11, Report of Investigations 6, 16 p.

Appendix A:
Data for Samples from Monitoring Wells

Chemical Data for Monitoring Well 2

Date	*24-Hr Time*	*Temp. (C)*	*pH*	*Eh (mV)*	*Specific Conductivity*	*Ca*	*Mg*	*Na*	*K*
4/16/91	1633	16.5	6.3	–	2360	386	171	19.4	14.1
7/17/91	1342	17.4	6.2	380	2600	342	188	12.4	11.0
10/23/91	1311	16.7	6.2	215	2860	398	206	21.2	14.0
2/5/92	1709	16.9	6.2	177	3230	414	244	17.8	12.6
n		4	4	3	4	4	4	4	4
max		17.4	6.3	380	3230	414	244	21.2	14.1
min		16.5	6.2	177	2360	342	171	12.4	11.0
avg		16.9		257	2760	385	202	17.7	12.9
std		0.4		108	373	31	31	3.8	1.5
CV (%)		2.3		42.1	13.5	8	15.5	21.5	11.3

Date	*Cl*	*Fe*	*F*	*Si*	*SO_4*	*HCO_3*	*Ba*	*Br*	TDS*
4/16/91	3.96	2.87	–	–	1230	584	0.02	< 1	2113
7/17/91	5.33	0.29	0.35	14.4	1270	439	0.05	< 1	2059
10/23/91	4.02	2.42	–	16.5	1360	598	0.09	–	2315
2/5/92	3.76	2.78	–	16.2	1620	559	0.02	–	2605
n	4	4	1	3	4	4	4	2	3
max	5.33	2.87	–	16.5	1620	598	0.09	–	2605
min	3.76	0.29	–	14.4	1230	439	0.02	–	2059
avg	4.27	2.09	–	15.7	1370	545	0.04	–	2273
std	0.72	1.21	–	1.1	175	72	0.03	–	247
CV (%)	16.8	58	–	7.2	12.8	13	70.1	–	11

*Total Dissolved Solids calculated, mg/L, with HCO_3 x 0.49 (Hem, 1985)
Specific conductivity in microsiemens
pH in Standard Units; all other units in mg/L
n=number of values min=minimum value std=standard deviation
max=maximum value avg=average value CV=coefficient of variation (percent)

Chemical Data for Monitoring Well 3

Date	*24-Hr Time*	*Temp. (C)*	*pH*	*Eh (mV)*	*Specific Conductivity*	*Ca*	*Mg*	*Na*	*K*
4/16/91	1754	16.3	6.05	–	2680	441	189	40.9	22.0
7/17/91	1515	18.6	6.25	370	2960	431	178	43.4	21.7
10/24/91	1315	18.1	6.18	296	3000	440	181	46.7	21.6
2/4/92	1050	17.2	6.31	278	3270	481	192	48.0	22.3
n		4	4	3	4	4	4	4	4
max		18.6	6.31	370	3270	481	192	48.0	22.3
min		16.3	6.05	278	2680	431	178	40.9	21,5
avg		17.6	–	315	2980	448	185	44,8	21,8
std		1	–	49	240	22	7	3.2	0.3
CV (%)		5.8	–	15.5	8.1	5	3.6	7.2	1.4

Date	*Cl*	*Fe*	*F*	*Si*	*SO_4*	*HCO_3*	*Ba*	*Br*	TDS*
4/16/91	7.18	1.37	–	bad	1330	763	0.22	< 1	2380
7/17/91	6.66	0.1	0.14	17.6	1320	738	0.02	< 1	2412
10/24/91	6.28	0.6	–	18.1	1330	749	0.02	–	2412
2/4/92	7.15	0.81	–	18.2	1510	756	0.02	–	2650
n	4	4	1	3	4	4	4	2	4
max	7.18	1.37	–	18.2	1510	763	0.22	–	2650
min	6.28	0.1	–	17.6	1320	738	0.02	–	2380
avg	6.82	0.72	–	18	1373	752	0.07	–	2463
std	0.43	0.53	–	0.3	92	11	0.1	–	125
CV (%)	6.3	73	–	1.8	6.7	1	138.1	–	5

*Total Dissolved Solids calculated, mg/L, with HCO_3 x 0.49 (Hem, 1985)
Specific conductivity in microsiemens
pH in Standard Units, all other units in Mg/L
n=number of values min=minimum value std=standard deviation
max=maximum value avg=average value CV=coefficient of variation (percent)

Chemical Data for Monitoring Well 4

Date	24-Hr Time	Temp. (C)	pH	Eh (mV)	Specific Conductivity	Ca	Mg	Na	K
4/16/91	1328	15.5	6.05	–	1080	75.6	60.8	45.8	4.3
7/17/91	1205	17.9	6.08	284	1300	96.8	73.7	40.1	5.0
10/23/91	1425	16.3	6.04	219	1230	90.4	69.0	28.7	4.9
2/4/92	1522	17.5	6.16	164	1350	99.0	77.1	19.4	4.2
6/16/92	1700	17.4	6.06	183	1210	88.4	68.0	17.4	4.0
n		5	5	4	5	5	5	5	5
max		17.9	6.16	284	1350	99.0	77.1	45.8	5.0
min		15.5	6.04	164	1080	75.6	60.8	17.4	4.0
avg		16.9	–	213	1240	90.0	69.7	30.3	4.5
std		1	–	53	101	9.2	6.2	12.5	0.4
CV (%)		5.9	–	24.8	8.2	10.2	8.9	41.3	9.7

Date	Cl	Fe	F	Si	SO_4	HCO_3	Ba	Br	TDS*
4/16/91	4	16.9	–	–	470	195	0.05	< 1	773
7/17/91	3	42.7	0.1	9.43	414	316	0.08	< 1	841
10/23/91	3	43.4	–	8.99	408	300	0.08	–	803
2/4/92	2	47.7	–	8.34	367	322	0.03	–	783
6/16/92	3	45.0	–	8.07	362	272	0.03	< 1	729
n	5	5	1	4	5	5	5	3	5
max	4	47.7	–	9.43	470	322	0.08	–	841
min	2	16.9	–	8.07	362	195	0.03	–	729
avg	3	39.1	–	8.71	404	281	0.05	–	789
std	1	12.6	–	0.62	44	52	0.03	–	47
CV (%)	23.4	32.1	–	7.09	10.8	18	48.3	–	6

*Total Dissolved Solids calculated, mg/L, with HCO_3 x 0.49 (Hem, 1985)
Specific conductivity in microsiemens
pH in Standard Units, all other units in mg/L
n=number of values min=minimum value std=standard deviation
max=maximum value avg=average value CV=coefficient of variation (percent)

Chemical Data for Monitoring Well 5

Date	24-Hr Time	Temp. (C)	pH	Eh (mV)	Specific Conductivity	Ca	Mg	Na	K
4/16/91	1440	18	6.1	–	2370	395	170	17.5	12.4
7/17/91	1425	19	6.5	361	2640	396	177	20.4	13.1
10/23/91	1539	19	6.2	311	2670	378	172	21.0	12.6
2/4/92	1402	19	6.3	256	2690	367	166	20.9	12.3
6/16/92	1620	19	6.2	313	2720	359	175	30.6	11.3
n		5	5	4	5	5	5	5	5
max		19.0	6.5	361	2720	396	177	30.6	13.1
min		18.0	6.1	256	2370	359	166	17.5	11.3
avg		18.4	–	310	2620	379	172	22.1	12.3
std		0.4	–	43	142	17	4	5.0	0.7
CV (%)		2.3	–	13.8	5.4	4.4	2.5	22.5	5.3

Date	Cl	Fe	F	Si	SO_4	HCO_3	Ba	Br	TDS*
4/16/91	4.6	1.46	–	–	1160	618	0.04	< 1	2064
7/17/91	4.1	0.07	0.12	17.7	1180	615	0.04	< 1	2109
10/23/91	4.6	0.26	–	17.5	1200	649	0.06	–	2124
2/4/92	4.4	0.26	–	15.5	1800	651	0.03	–	2705
6/16/92	8.2	0.06	–	15.7	1160	647	0.03	< 1	2077
n	5	5	1	4	5	5	5	3	5
max	8.2	1.46	–	17.7	1200	651	0.06	–	2705
min	4.1	0.06	–	15.5	1160	615	0.03	–	2064
avg	5.2	0.42	–	16.6	1176	636	0.04	–	2216
std	1.7	0.59	–	1.2	17	18	0.01	–	275
CV (%)	32.9	139.8	–	7.0	1.4	3.0	25.9	–	12

*Total Dissolved Solids calculated, mg/L, with HCO_3 x 0.49 (Hem, 1985)
Specific conductivity in microsiemens
pH in Standard Units, all other units in mg/L
n=number of values min=minimum value std=standard deviation
max=maximum value avg=average value CV=coefficient of variation (percent)

Chemical Data for Monitoring Well 6

Date	24-Hr Time	Temp. (C)	pH	Eh (mV)	Specific Conductivity	Ca	Mg	Na	K
4/17/91	1020	16.8	6.19	–	1020	106	62.2	4.42	5.8
7/18/91	946	17.8	5.88	357	929	92	60.9	4.82	6.8
10/23/91	1630	17.5	5.85	273	1040	93	67.9	5.38	7.2
2/5/92	1245	15.2	5.58	209	1140	104	71.6	4.64	6.6
6/16/92	1530	18.2	5.91	273	1090	101	73.5	4.81	3.5
n		5	5	4	5	5	5	5	5
max		18.2	6.19	357	1140	106	73.5	5.38	7.2
min		15.2	5.58	209	929	92	60.9	4.42	3.5
avg		17.1	–	278	1040	99	67.2	4.81	6.0
std		1.2	–	60	80	6	5.6	0.36	1.5
CV (%)		6.9	–	21.7	7.7	6.4	8.3	7.4	24.9

Date	Cl	Fe	F	Si	SO_4	HCO_3	Ba	Br	TDS*
4/17/91	3.23	2.36	–	–	327	214	0.02	< 1	616
7/18/91	4.64	6.51	0.16	6.58	346	185	0.02	< 1	619
10/23/91	2.26	5.93	–	6.32	381	216	0.03	–	675
2/5/92	2.11	4.48	–	5.56	380	249	0.02	–	701
6/16/92	3.02	5.58	–	6.93	348	251	0.02	< 1	669
n	5	5	1	4	5	5	5	3	5
max	4.64	6.51	–	6.93	381	251	0.03	–	701
min	2.11	2.36	–	5.56	327	185	0.02	–	616
avg	3.05	4.97	–	6.35	356	223	0.02	–	656
std	1.01	1.64	–	0.58	23	27	0.01	–	37
CV (%)	33.1	32.9	–	9.16	6.6	12	23.4	–	6

*Total Dissolved Solids calculated, mg/L, with HCO_3 x 0.49 (Hem, 1985)
Specific conductivity in microsiemens
pH in Standard Units, all other units in mg/L
n=number of values min=minimum value std=standard deviation
max=maximum value avg=average value CV=coefficient of variation (percent)

Chemical Data for Monitoring Well 7

Date	24-Hr Time	Temp. (C)	pH	Eh (mV)	Specific Conductivity	Ca	Mg	Na	K
4/17/91	1115	18	6.5	–	3100	286	292	30.6	16.5
7/18/91	1029	20	6.39	198	2990	284	270	39.2	15.3
10/24/91	1558	19	6.37	131	3500	339	313	40.6	13.8
2/5/92	1156	16	6.35	111	3390	284	314	30.7	15.9
6/15/92	1505	19	6.54	196	3210	299	318	41.7	10.5
n		5	5	4	5	5	5	5	5
max		20	6.54	198	3500	339	318	41.7	16.5
min		16	6.35	111	2990	284	270	30.6	10.5
avg		18	–	159	3240	298	301	36.6	14.4
std		2	–	45	206	24	20	5.5	2.4
CV (%)		8.5	–	28.1	6.4	7.9	6.7	15	16.7

Date	Cl	Fe	F	Si	SO_4	HCO_3	Ba	Br	TDS*
4/17/91	5.5	31.3	–	–	1140	805	0.04	< 1	2196
7/18/91	6.5	42.9	0.18	17.3	1320	726	0.05	< 1	2351
10/24/91	6.9	69.0	–	21.8	1960	630	0.03	–	3073
2/5/92	5.8	29.9	–	14.1	1300	1046	0.03	–	2507
6/15/92	7.3	47.6	–	19.5	1680	645	0.09	< 1	2740
n	5	5	1	4	5	5	5	3	5
max	7.3	69.0	–	21.8	1960	1046	0.09	–	3073
min	5.5	29.9	–	14.1	1140	630	0.03	–	2196
avg	6.4	44.1	–	18.2	1480	770	0.05	–	2573
std	0.7	15.8	–	3.3	333	169	0.03	–	344
CV (%)	11.6	35.8	–	18.0	22.5	22	54.4	–	13

*Total Dissolved Solids calculated, mg/L, with HCO_3 x 0.49 (Hem, 1985)
Specific conductivity in microsiemens
pH in Standard Units, all other units in mg/L
n=number of values min=minimum value std=standard deviation
max=maximum value avg=average value CV=coefficient of variation (percent)

Chemical Data for Monitoring Well 8

Date	24-Hr Time	Temp. (C)	pH	Eh (mV)	Specific Conductivity	Ca	Mg
4/16/91	1830	18.2	6.09	–	3290	539	199
7/17/91	1630	20.4	6.35	298	3370	509	186
10/24/91	1433	20.4	6.39	213	3340	443	182
2/5/92	1337	17.8	6.15	174	3720	476	193
6/15/92	1720	19.8	6.22	223	3100	458	196
n		5	5	4	5	5	5
max		20.4	6.39	298	3720	539	199
min		17.8	6.09	174	3100	443	182
avg		19.3	–	227	3360	485	191
std		1.2	–	52	226	39	7
CV (%)		6.4	–	22.9	6.7	8	3.7

Date	Na	K	Cl	Fe	F	Si	SO_4
4/16/91	118.0	25.0	11.9	7.89	–	–	1780
7/17/91	93.4	24.6	9.1	5.12	0.24	20	1590
10/24/91	95.8	23.4	8.3	5.61	–	18	1560
2/5/92	90.9	22.9	8	5.96	–	18	1600
6/15/92	83.0	20.3	8.6	6.96	–	19	1750
n	5	5	5	5	1	4	5
max	118.0	25.0	11.9	7.89	–	20	1780
min	83.0	20.3	8	5.12	–	18	1560
avg	95.8	23.2	9.2	6.31	–	19	1656
std	13.1	1.9	1.6	1.11	–	1	101
CV (%)	13.6	8	17.4	17.6	–	5	6.1

Date	HCO_3	Alkalinity as $CaCO_3$	Ba	Br	TDS*
4/16/91	727	–	0.02	< 1	3037
7/17/91	742	608	0.02	< 1	2801
10/24/91	749	614	0.02	–	2703
2/5/92	769	630	0.02	–	2792
6/15/92	736	603	0.02	< 1	2902
n	5	4	5	3	5
max	786	630	0.23	–	3037
min	727	603	0.02	–	2703
avg	744.42	614	0.02	–	2847
std	15.76	12	0	–	128
CV (%)	2.1	1.9	14.9	–	4

*Total Dissolved Solids calculated, mg/L, with HCO_3 x 0.49 (Hem, 1985)
Specific Conductivity in microsiemens
pH in Standard Units, all other units in mg/L
min=minimum value std=standard deviation
max=maximum value avg=average value
n=number of values CV=coefficient of variation (percent)

Chemical Data for Monitoring Well 9

Date	24-Hr Time	Temp. (C)	pH	Eh (mV)	Specific Conductivity	Ca	Mg
4/17/91	1345	19.5	6.2	–	3160	441	233
7/17/91	1719	20.3	6.2	339	2890	439	222
10/24/91	1730	19.7	6.3	211	2790	352	215
2/4/92	1408	18.9	6.3	264	2770	325	196
6/16/92	1427	21.8	6.2	285	2440	284	178
n		5	5	4	5	5	5
max		21.8	6.3	339	3160	441	233
min		18.9	6.2	211	2440	284	178
avg		20	–	275	2810	368	209
std		1.1	–	53	258	70	22
CV (%)		5.5	–	19.2	9.2	19	10.5

Date	Na	K	Cl	Fe	F	Si	SO_4
4/17/91	20.3	17.5	7.65	1.24	–	–	1510
7/17/91	19.3	17.9	6.2	0.88	0.16	17.7	1290
10/24/91	20.1	17.3	6.53	0.99	–	15.6	1260
2/4/92	18.3	15.5	5.73	1.07	–	12.3	1150
6/16/92	16.0	12.3	6.77	0.56	–	13.1	806
n	5	5	5	5	1	4	5
max	20.3	17.9	7.65	1.24	–	17.7	1510
min	16.0	12.3	5.73	0.56	–	12.3	806
avg	18.8	16.1	6.58	0.95	–	14.7	1203
std	1.8	2.3	0.72	0.26	–	2.5	258
CV (%)	9.3	14.4	10.9	26.9	–	16.8	21.4

Date	HCO_3	Alkalinity as $CaCO_3$	Ba	Br	TDS*
4/17/91	580	–	0.02	< 1	2515
7/17/91	653	535	0.02	< 1	2333
10/24/91	649	532	0.03	–	2205
2/4/92	673	552	0.02	–	2053
6/16/92	649	532	0.02	< 1	1635
n	5	4	5	3	5
max	673	552	0.03	–	2515
min	580	532	0.02	–	1635
avg	641	538	0.02	–	2057
std	36	10	0.00	–	304
CV (%)	5.5	1.8	17.3	–	14.8

*Total Dissolved Solids calculated, mg/L, with HCO_3 x 0.49 (Hem, 1985)
Specific Conductivity in microsiemens
pH in Standard Units, all other units in mg/L
min=minimum value
max=maximum value
n=number of values
std=standard deviation
avg=average value
CV=coefficient of variation (percent)

Chemical Data for Monitoring Well 10

Date	24-Hr Time	Temp. (C)	pH	Eh (mV)	Specific Conductivity	Ca	Mg
4/17/91	1225	15.8	6.2	–	2410	316	190
7/18/91	1200	17.4	6.12	330	2480	302	194
10/24/91	1520	17.9	6.21	250	2720	307	224
2/4/92	1027	15.6	6.24	308	2500	287	184
6/15/92	1500	18.4	6.27	292	2390	303	205
8/10/94	–	–	–	–	–	301	219
n		5	5	4	5	6	6
max		18.4	6.27	330	2720	316	224
min		15.6	6.12	250	2390	287	184
avg		17.0	–	295	2500	303	203
std		1.3	–	34	131	9	16
CV (%)		7.4	–	11	5	3	8

Date	Na	K	Cl	Fe	F	Si	SO_4
4/17/91	12.8	12.7	4.7	0.35	–	bad	1060
7/18/91	13.8	12.7	5.52	< 0.004	0.2	13.4	1120
10/24/91	16	13.0	5.32	1.09	–	14.2	1300
2/4/92	13.7	12.4	4.88	0.06	–	11.8	1000
6/15/92	15.5	11.6	6.36	0.04	–	13.8	1100
8/10/94	15.3	13.1	8.3	0.239	–	–	1270
n	6	6	6	6	1	4	6
max	16.0	13.1	8.3	1.09	–	14.2	1300
min	12.8	11.6	4.7	< 0.004	–	11.8	1000
avg	14.5	12.5	–	–	–	13.3	1142
std	1.3	0.5	–	–	–	1.1	119
CV (%)	8.7	4.3	–	–	–	7.9	10

Date	HCO_3	Alkalinity as $CaCO_3$	Ba	Br	TDS*
4/17/91	519	–	0.02	< 1	1851
7/18/91	551	452	0.01	< 1	1932
10/24/91	565	463	0.02	–	2157
2/4/92	577	473	0.02	–	1797
6/15/92	595	488	0.02	< 1	1947
8/10/94	583	478	0.026	<1	2113
n	6	5	6.00	3	6
max	595	488	0.03	–	2157
min	519	452	0.01	–	1797
avg	565	470.8	0.02	–	1966
std	27.1	13.8	0.0	–	142
CV (%)	4.80	2.94	26.7	–	14

*Total Dissolved Solids calculated, mg/L, with HCO_3 x 0.49 (Hem, 1985)
Specific Conductivity in microsiemens
pH in Standard Units, all other units in mg/L
min=minimum value std=standard deviation n=number of values
max=maximum value CV=coefficient of variation (%) avg=average value

Chemical Data for Monitoring Well 11

Date	24-Hr Time	Temp. (C)	pH	Eh (mV)	Specific Conductivity	Ca	Mg
4/17/91	1630	20	6.33	–	3990	567	321
7/17/91	1908	21	6.22	223	3700	497	304
10/24/91	1020	20	5.88	204	3590	465	299
2/4/92	1137	21	6.58	140	3750	450	278
6/16/92	1150	22	6.35	183	3390	447	285
n		5	5	4	5	5	5
max		22	6.58	223	3990	567	321
min		20	5.88	140	3390	447	278
avg		21	–	188	3690	485	297
std		1	–	36	221	50	17
CV (%)		3.7	–	19.1	6	10.3	5.7

Date	Na	K	Cl	Fe	F	Si	SO_4
4/17/91	32.5	21.7	9	5	–	–	1900
7/17/91	29.2	20.6	10	24	0.16	22.3	1940
10/24/91	29.8	19.5	10	10	–	21.1	1920
2/4/92	27.5	18.1	8	11	–	19.2	1780
6/16/92	29.2	19.0	10	12	–	21.3	1680
n	5	5	5	5	1	4	5
max	32.5	21.7	10	24	–	22.3	1940
min	27.5	18.1	8	5	–	19.2	1680
avg	29.6	19.8	9	12	–	21.0	1844
std	1.8	1.4	1	7	–	1.3	111
CV (%)	6.1	7.1	11.9	54.8	–	6.2	6.0

Date	HCO_3	Alkalinity as $CaCO_3$	Ba	Br	TDS*
4/17/91	739	–	0.03	< 1	3219
7/17/91	773	634	0.03	< 1	3226
10/24/91	786	644	0.04	–	3160
2/4/92	817	670	0.03	–	2992
6/16/92	855	701	0.03	< 1	2922
n	5	4	5	3	5
max	855	701	0.04	–	3226
min	739	634	0.03	–	2922
avg	794	662	0.03	–	3104
std	44	30	0.00	–	139
CV (%)	5.6	4.5	10.8	–	4

*Total Dissolved Solids calculated, mg/L, with HCO_3 x 0.49 (Hem, 1985)
Specific Conductivity in microsiemens
pH in Standard Units, all other units in mg/L
min=minimum value std=standard deviation
max=maximum value avg=average value
n=number of values CV=coefficient of variation (percent)

Chemical Data for Monitoring Well 12

Date	24-Hr Time	Temp. (C)	pH	Eh (mV)	Specific Conductivity	Ca	Mg
4/17/91	1715	18	6.38	–	2830	463	151
7/18/91	1407	18	6.25	281	3150	510	169
10/24/91	1355	18	6.13	266	3370	483	189
2/4/92	1007	17	6.3	282	3310	481	179
6/16/92	1030	20	6.43	250	2930	466	184
n		5	5	4	5	5	5
max		20	6.43	282	3370	510	189
min		17	6.13	250	2830	463	151
avg		18	–	270	3120	481	174
std		1	–	15	235	19	15
CV (%)		6.4	–	5.6	7.5	3.9	8.6

Date	Na	K	Cl	Fe	F	Si	SO_4
4/17/91	43.2	19.1	5.2	2.97	–	–	1160
7/18/91	53.2	19.5	6.4	1.55	0.12	18.6	1480
10/24/91	46.1	18.9	7.3	1.83	–	18.5	1620
2/4/92	60.9	19.4	6.4	1.61	–	17.2	1360
6/16/92	59.1	18.9	7.6	2.08	–	18.7	1440
n	5	5	5	5	1	4	5
max	60.9	19.5	7.6	2.97	–	18.7	1620
min	43.2	18.9	5.2	1.55	–	17.2	1160
avg	52.5	19.2	6.6	2.01	–	18.3	1412
std	7.8	0.3	1.0	0.58	–	0.7	169
CV (%)	14.8	1.5	14.6	28.7	–	3.9	12.0

Date	HCO_3	Alkalinity as $CaCO_3$	Ba	Br	TDS*
4/17/91	729	–	0.02	< 1	2202
7/18/91	686	562	0.01	< 1	2595
10/24/91	725	594	0.01	–	2740
2/4/92	720	590	0.02	–	2478
6/16/92	711	583	0.02	< 1	2545
n	5	4	5	3	5
max	729	594	0.02	–	2740
min	686	562	0.01	–	2202
avg	714	582	0.02	–	2512
std	17	14	0.01	–	198
CV (%)	2.4	2.5	34.8	–	7.9

*Total Dissolved Solids calculated, mg/L, with HCO_3 x 0.49 (Hem, 1985)
Specific Conductivity in microsiemens
pH in Standard Units, all other units in mg/L
min=minimum value
max=maximum value
n=number of values
std=standard deviation
avg=average value
CV=coefficient of variation (percent)

Chemical Data for Monitoring Well 13

Date	24-Hr Time	Temp. (C)	pH	Eh (mV)	Specific Conductivity	Ca	Mg
4/17/91	1440	17	6.23	–	2760	413	205
7/17/91	1810	18	6.16	311	2830	426	209
10/24/91	1158	20	6.14	243	2890	379	212
2/4/92	1335	18	6.32	240	2960	395	212
6/15/92	1812	19	6.23	226	2560	396	228
n		5	5	4	5	5	5
max		20	6.32	311	2960	426	228
min		17	6.14	226	2560	379	205
avg		18	–	255	2800	402	213
std		1	–	38	155	18	9
CV (%)		6.3	–	14.9	5.5	4.5	4.1

Date	Na	K	Cl	Fe	F	Si	SO_4
4/17/91	19.3	11.9	6.1	11.3	–	–	1370
7/17/91	20.3	13.2	10.1	5.5	0.16	17.5	1350
10/24/91	23.3	11.9	7.7	8.5	–	17.3	1340
2/4/92	22.8	12.3	8.3	10.3	–	18.2	1280
6/15/92	25.9	10.1	8.9	7.5	–	18.5	1440
n	5	5	5	5	1	5	5
max	25.9	13.2	10.1	11.3	–	18.5	1440
min	19.3	10.1	6.1	5.5	–	17.3	1280
avg	22.3	11.9	8.2	8.6	–	17.9	1356
std	2.6	1.1	1.5	2.3	–	0.6	58
CV (%)	11.7	9.5	18.0	26.7	–	3.2	4.3

Date	HCO_3	Alkalinity as $CaCO_3$	Ba	Br	TDS*
4/17/91	483	–	0.019	< 1	2273
7/17/91	597	489	0.010	< 1	2344
10/24/91	586	480	0.019	–	2287
2/4/92	614	503	0.060	–	2260
6/15/92	586	480	0.018	< 1	2422
n	5	4	5	3	5
max	614	503	0.060	–	2422
min	483	480	0.010	–	2260
avg	573	488	0.025	–	2317
std	52	11	0.020	–	67
CV (%)	9.0	2.2	79.4	–	2.9

*Total Dissolved Solids calculated, mg/L, with HCO_3 x 0.49 (Hem, 1985)
Specific Conductivity in microsiemens
pH in Standard Units, all other units in mg/L
min=minimum value
max=maximum value
n=number of values
std=standard deviation
avg=average value
CV=coefficient of variation (percent)

Chemical Data for Monitoring Well 14

Date	24-Hr Time	Temp. (C)	pH	Eh (mV)	Specific Conductivity	Ca	Mg
4/17/91	1545	18	4.18	–	1321	111	84
7/18/91	1313	19	4.14	393	1500	152	96
10/24/91	1115	18	4.22	412	1480	143	100
2/4/92	1255	19	4.26	383	1640	157	101
6/16/92	1305	20	4.33	405	1560	149	106
n		5	5	4	5	5	5
max		20	4.33	412	1640	157	106
min		18	4.14	383	1321	111	84
avg		19	–	398	1500	142	97
std		1	–	13	116	18	8
CV (%)		4.3	–	3.3	7.7	12.8	8.6

Date	Na	K	Cl	Fe	F	Si	SO_4
4/17/91	12.1	3.6	7.2	8.81	–	–	695
7/17/91	12.0	3.4	7.7	5.58	1.06	14	785
10/24/91	13.4	3.8	7.4	5.75	–	13	873
2/4/92	13.1	3.5	7.2	4.98	–	12	857
6/15/92	14.5	1.6	7.7	5.59	–	14	827
n	5	5	5	5	1	4	5
max	14.5	3.8	7.7	8.81	–	14	873
min	12.0	1.6	7.2	4.98	–	5	695
avg	13.0	3.2	7.4	6.14	–	12	807
std	1.0	0.9	0.3	1.52	–	4	71
CV (%)	7.9	28.1	3.6	24.8	–	31.6	8.8

Date	HCO_3	Alkalinity as $CaCO_3$	Ba	Br	TDS*
4/17/91	3.66	–	0.04	< 1	924
7/17/91	3.66	3	0.03	< 1	1078
10/24/91	8.54	7	0.04	–	1163
2/4/92	4.88	4	0.03	–	1159
6/15/92	3.66	3	0.03	< 1	1128
n	5	4	5	3	5
max	8.54	7	0.04	–	1163
min	3.66	3	0.03	–	924
avg	4.88	4	0.03	–	1090
std	2.11	2	0.01	–	99
CV (%)	43.3	44.5	18.7	–	9.1

*Total Dissolved Solids calculated, mg/L, with HCO_3 x 0.49 (Hem, 1985)
Specific Conductivity in microsiemens
pH in Standard Units, all other units in mg/L
min=minimum value
max=maximum value
n=number of values
std=standard deviation
avg=average value
CV=coefficient of variation (percent)

Chemical Data for Spring 1

Date	24-Hr Time	Temp. (C)	pH	Eh (mV)	Specific Conductivity	Ca	Mg
4/17/91	1124	14	6.35	–	1740	197	123
7/18/91	1122	18	6.16	325	1970	267	144
10/24/91	1650	17	6.17	320	2680	336	189
2/5/92	1121	13	6.06	333	2400	274	160
6/15/92	1850	15	6.05	348	1880	275	169
6/15/92	1850	13	6.41	0	2430	240	164
n		5	5	4	5	5	5
max		18	6.35	348	2680	336	189
min		13	6.05	320	1740	197	123
avg		15	–	332	2140	270	157
std		2.1	–	12	390	49	25
CV (%)		13.5	–	3.7	18.3	18.3	15.9

Date	Na	K	Cl	Fe	F	Si	SO_4
4/17/91	20.9	9.6	5.6	1.16	–	–	779
7/17/91	22.8	11.7	5.0	0.05	0.2	12	842
10/24/91	37.2	15.0	7.3	0.08	–	14	1300
2/4/92	27.4	11.6	5.5	< 0.004	–	11	1020
6/15/92	27.7	10.6	6.5	< 0.004	–	12	976
6/10/94	20.2	10.5	6.1	< 0.006	–	11	1020
n	5	5	5	5	1	14	5
max	37.2	15.0	7.3	1.16	–	11	1300
min	20.9	9.6	5.0	–	–	12	779
avg	27.2	11.7	6.0	–	–	1	983
std	6.3	2.0	0.9	–	–	10	202
CV (%)	23.2	17.3	14.7	–	–	41.2	20.6

Date	HCO_3	Alkalinity as $CaCO_3$	Ba	Br	TDS*
4/17/91	454	–	0.02	< 1	1359
7/17/91	401	329	0.02	< 1	1502
10/24/91	578	474	0.02	–	2182
2/4/92	476	390	0.02	–	1743
6/15/92	468	384	0.02	< 1	1707
6/10/94	452	–	0.02	< 1	1694
max	578	474	0.02	–	2182
min	401	329	0.02	–	1359
avg	476	394	0.02	–	1698
std	64	60	0.00	–	279
CV (%)	13.5	15.2	11.4	–	16.4

*Total Dissolved Solids calculated, mg/L, with HCO_3 x 0.49 (Hem, 1985)
Specific Conductivity in microsiemens
pH in Standard Units, all other units in mg/L
min=minimum value std=standard deviation
max=maximum value avg=average value
n=number of values CV=coefficient of variation (%)

Chemical Data for Pond Overflow 1

Date	*24-Hr Time*	*Temp (C)*	*pH*	*Eh (mV)*	*Specific Conductivity*	*Ca*	*Mg*
6/10/94	1059	23	7	–	3110	328	222

Date	*Na*	*K*	*Cl*	*Fe*	*F*	*Si*	*SO_4*
6/10/94	27.1	15.3	7.9	< 0.006	–	15.6	1350

Date	*HCO_3*	*Alkalinity as $CaCO_3$*	*Ba*	*Br*	*TDS**
6/10/94	657	–	0.022	–	2280

*Total Dissolved Solids calculated, mg/L, with HCO_3 x 0.49 (Hem, 1985)
Specific Conductivity in microsiemens
pH in Standard Units, all other units in mg/L

min=minimum value	std=standard deviation
max=maximum value	avg=average value
n=number of values	CV=coefficient of variation (percent)

Chemical Data for Long Fork Flume

Date	*24-Hr Time*	*Temp (C)*	*pH*	*Eh (mV)*	*Specific Conductivity*	*Ca*	*Mg*
6/10/94	–	18	7.56	–	2650	277	197

Date	*Na*	*K*	*Cl*	*Fe*	*F*	*Si*	*SO_4*
6/10/94	20.1	12.6	6.4	< 0.006	–	12.9	1180

Date	*HCO_3*	*Alkalinity as $CaCO_3$*	*Ba*	*Br*	*TDS**
6/10/94	491	–	0.028	–	1947

*Total Dissolved Solids calculated, mg/L, with HCO_3 x 0.49 (Hem, 1985)
Specific Conductivity in microsiemens
pH in Standard Units, all other units in mg/L

min=minimum value	std=standard deviation
max=maximum value	avg=average value
n=number of values	CV=coefficient of variation (percent)

Chemical Data for Chestnut Gap Branch

Date	24-Hr Time	Temp (C)	pH	Eh (mV)	Specific Conductivity	Ca	Mg
6/10/94	1059	22	8.11	–	830	67.6	49.8

Date	Na	K	Cl	Fe	F	Si	SO_4
6/10/94	6.49	5.1	3.9	0.044	–	4.66	350

Date	HCO_3	Alkalinity as $CaCO_3$	Ba	Br	TDS*
6/10/94	185	–	0.034	–	579

*Total Dissolved Solids calculated, mg/L, with HCO_3 x 0.49 (Hem, 1985)
Specific Conductivity in microsiemens
pH in Standard Units, all other units in mg/L

min=minimum value	std=standard deviation
max=maximum value	avg=average value
n=number of values	CV=coefficient of variation (percent)

Appendix B:
Data for Storm-Event Sampling

Percentage of Precipitation Measured as Runoff During Storm Events at the Star Fire site. Modified from Taylor (1995).					
	Precipitation		*Observed Runoff*		
*Date**	*(Inches)*	*(Acre-Ft)*	*(Inches)*	*(Acre-Ft)*	*% Precipitation as Runoff*
6/9/90a	0.46	0.72	0.06	0.10	13.80
6/9/90b	0.92	1.45	0.19	0.30	20.70
6/14/90	0.52	0.82	0.03	0.04	4.88
6/20/90	1.70	2.68	0.33	0.52	19.42
6/22/90	0.31	0.49	0.03	0.04	8.19
7/11/90	0.63	0.99	0.02	0.03	3.02
7/13/90a	1.60	2.52	0.03	0.04	1.59
7/13/90b	2.32	3.65	0.19	0.30	8.21
7/14/90	0.37	0.58	0.04	0.07	12.01
7/23/90	0.31	0.49	0.01	0.01	2.05
7/30/90	0.63	0.99	0.08	0.12	12.09
8/4/90	0.35	0.55	0.03	0.04	7.26
8/5/90	0.90	1.42	0.12	0.19	13.40
8/8/90	1.03	1.62	0.08	0.12	7.40
8/29/90	0.70	1.10	0.07	0.11	9.98
9/9/90	0.79	1.24	0.17	0.26	20.90
9/12/90	0.39	0.61	0.04	0.06	9.77
9/19/90	0.77	1.21	0.01	0.01	0.82
9/22/90	0.72	1.13	0.05	0.08	7.05
10/22/90	0.79	1.24	0.06	0.09	7.23
11/5/90	0.33	0.52	0.04	0.07	13.47
11/9/90	0.59	0.93	0.01	0.02	2.15
12/3/90	0.85	1.34	0.17	0.26	19.42
12/30/90	0.98	1.54	0.34	0.53	34.34
3/22/91	0.96	1.51	0.29	0.46	30.42
3/29/91	0.92	1.45	0.18	0.28	19.32
4/15/91	0.79	1.24	0.15	0.24	19.29
5/29/91	1.64	2.58	0.36	0.56	21.68
6/1/91	0.74	1.17	0.13	0.21	18.02
6/2/91	0.24	0.38	0.01	0.01	2.65
6/3/91	1.18	1.86	0.32	0.50	26.90
6/18/91	0.28	0.44	0.01	0.01	2.27
6/22/91a	1.05	1.65	0.16	0.25	15.12
6/22/91b	0.79	1.24	0.10	0.16	12.86
6/25/91	1.05	1.65	0.10	0.15	9.07
7/5/91	1.40	2.21	0.17	0.27	12.24
7/10/91	0.53	0.83	0.04	0.07	8.39
7/13/91	0.37	0.58	0.01	0.02	3.43
7/23/91	1.20	1.89	0.07	0.11	5.82
8/7/91	0.92	1.45	0.13	0.20	13.80
8/9/91	1.49	2.35	0.22	0.35	14.91
9/17/91	0.70	1.10	0.04	0.06	5.44
					Avg. 11.92
*Letters after dates indicate more than one sample gathered on those dates.					